Volume 11
Number 12
December 2020
Pages 1329–1430

RSC Medicinal Chemistry

rsc.li/medchem

ISSN 2632-8682

ROYAL SOCIETY OF CHEMISTRY

RESEARCH ARTICLE
Kevin Kavanagh, Trinidad Velasco-Torrijos *et al.*
Scaffold diversity for enhanced activity of glycosylated inhibitors of fungal adhesion

RSC Medicinal Chemistry

ROYAL SOCIETY OF CHEMISTRY

RESEARCH ARTICLE

Cite this: *RSC Med. Chem.*, 2020, **11**, 1386

Scaffold diversity for enhanced activity of glycosylated inhibitors of fungal adhesion†

Harlei Martin,[a] Tara Somers,[b] Mathew Dwyer,[b] Ryan Robson,[c] Frederick M. Pfeffer,[c] Ragnar Bjornsson,[d] Tobias Krämer,[ae] Kevin Kavanagh*[bf] and Trinidad Velasco-Torrijos*[af]

Received 29th June 2020,
Accepted 11th August 2020

DOI: 10.1039/d0md00224k

rsc.li/medchem

Candida albicans is one of the most prevalent fungal pathogens involved in hospital acquired infections. It binds to glycans at the surface of epithelial cells and initiates infection. This process can be blocked by synthetic carbohydrates that mimic the structure of cell surface glycans. Herein we report the evaluation of a series of divalent glycosides featuring aromatic (benzene, squaramide) and bicyclic aliphatic (norbornene) scaffolds, with the latter being the first examples of their kind as small molecule anti-adhesion glycoconjugates. Galactosides **1** and **6**, built on an aromatic core, were most efficient inhibitors of adhesion of *C. albicans* to buccal epithelial cells, displacing up to 36% and 48%, respectively, of yeast already attached to epithelial cells at 138 μM. Remarkably, *cis-endo*-norbornene **21** performed comparably to benzene-core derivatives. Conformational analysis reveals a preference for compounds **1** and **21** to adopt folded conformations. These results highlight the potential of norbornenes as a new class of aliphatic scaffolds for the synthesis of anti-adhesion compounds.

Introduction

The adhesion of pathogens to the surface of the host cell is the first step in infection. The inhibition of this critical process is an attractive strategy in the quest for new anti-infection agents.[1] Adhesins, the proteins that mediate attachment to the host cell surface, have thus become important therapeutic targets.[2] The precise structure of a number of adhesins has been established through crystallographic studies,[3–6] aiding the design of high affinity ligands aimed at blocking the adhesion processes in microbial pathogens such as *Pseudomonas aeruginosa*, *Aspergillus fumigatus* or *Escherichia coli*.[7–12] Unfortunately, for many adhesins detailed structural information is unavailable, thus the search for inhibitors usually proceeds through library screening.[13,14]

Candida albicans is known to cause a variety of diseases in immunocompromised patients, and this opportunistic yeast is now recognised as a major threat to hospitalized individuals.[15,16] The yeast causes infection by binding to host cells and colonizing mucosal epithelia.[17,18] The adhesion processes for *C. albicans* are complex and involve both (i) non-specific hydrophobic binding and (ii) specific adhesin mediated interactions.[19–22] Adhesins in *Candida* species are often lectins[23] that recognize cell surface glycans containing terminal galactose,[24–26] fucose[27] and *N*-acetyl glucosamine.[28] However, there are very few X-ray crystallographic studies that can provide detailed structural information on the mode of binding of fungal lectins[25,26,29] and importantly, none specifically refer to *C. albicans* carbohydrate-binding adhesins.

We have previously reported the synthesis of a small library of glycoconjugates and their evaluation as inhibitors of the adherence of *C. albicans* to buccal epithelial cells (BECs); we identified divalent galactoside **1**, with a triazolyl group directly linked to the anomeric position, as a very effective inhibitor of fungal adhesion, displacing over 50% of *C. albicans* cells already attached to BECs (Fig. 1a).[30] We found that the spatial presentation of the carbohydrate epitopes strongly influenced the biological activity: addition of the *O*-ethylene linker in **2** slightly decreased anti-adhesion ability, while the replacement of galactosides by lactosides in **3** led to increased adhesion between fungal and epithelial cells. These results highlighted the critical role of structural elements, such as linkers, in providing appropriate orientation of the carbohydrate motifs. In the present work, we focus on the molecular scaffolds onto which the

[a] *Department of Chemistry, Maynooth University, Maynooth, Co. Kildare, Ireland. E-mail: trinidad.velascotorrijos@mu.ie*
[b] *Department of Biology, Maynooth University, Maynooth, Co. Kildare, Ireland*
[c] *School of Life and Environmental Sciences, Deakin University, Geelong, Victoria 3217, Australia*
[d] *Department of Inorganic Spectroscopy, Max Planck Institute for Chemical Energy Conversion, Stiftstrasse 34–36, 45470 Mülheim an der Ruhr, Germany*
[e] *The Hamilton Institute, Maynooth University, Maynooth, Co. Kildare, Ireland*
[f] *The Kathleen Lonsdale Institute for Human Health Research, Maynooth University, Maynooth, Co. Kildare, Ireland*

† Electronic supplementary information (ESI) available. See DOI: 10.1039/d0md00224k

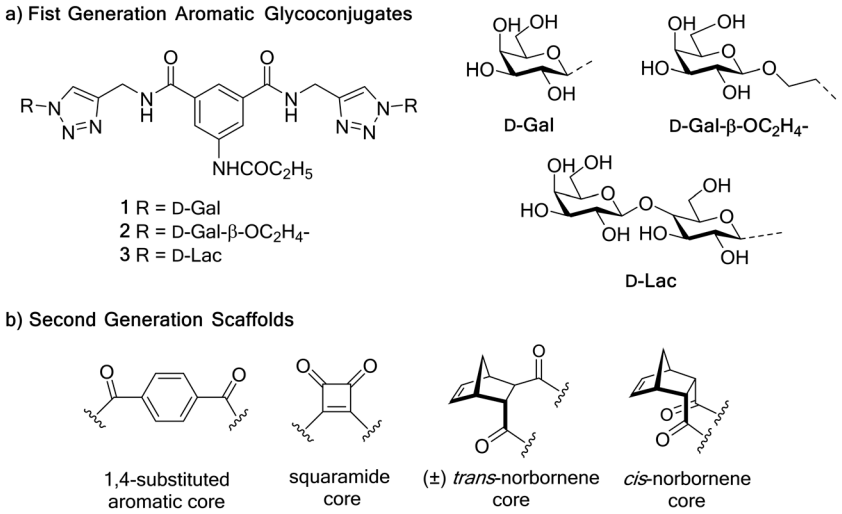

Fig. 1 a) Chemical structures of selected aromatic-core glycoconjugates evaluated as inhibitors of adhesion of opportunistic yeast *C. albicans*.;[30] b) Structures of the core scaffolds used in the synthesis of a second-generation anti-adhesion ligands.

recognition epitopes are installed to approach the optimization of lead compound **1**. As the protein target of **1** is not known, structure-guided design strategies to enhance affinity are not possible; as such, we investigated new core scaffolds that can orient both galactosyl moieties in comparable three-dimensional arrangement to lead compound **1**. Although benzene derivatives remain extremely popular in the design of bioactive compounds, their replacement with saturated bicyclic structures has recently emerged in medicinal chemistry as a powerful strategy to access new compounds with improved biological and physicochemical properties.[31] Herein, we compare bicyclic aliphatic (norbornenes) molecular scaffolds with aromatic ones (benzene, squaramides), with the former being used for the first time in the synthesis of small molecule anti-adhesion glycoconjugates (Fig. 1).

Results and discussion

Synthesis

As our original study focused on glycoconjugates built around aromatic scaffolds with either a 1,3 or 1,3,5 substitution pattern we decided to first explore 1,4 substituted analogues of lead compound **1**. Thus, terephthalic acid was reacted with propargyl amine using freshly prepared 4-(4,6-dimethoxy-1,3,5-triazin-2-yl)-4-methylmorpholinium chloride (DMTMM,[32]) to give diamide **4**[33] in 81% yield (Scheme 1). Next, **4** was reacted with 2,3,4,6-tetra-*O*-acetyl-1-β-azido-D-galactopyranoside[34] using microwave mediated copper-catalyzed azide–alkyne cycloaddition (CuAAC) methodology, to give protected compound **5** in 73% yield. Deacetylation was accomplished under mild basic conditions to give the desired diglycoside **6** in excellent yield (94%).

Squaramides, due to their ability to act as effective hydrogen bond donors, have been extensively investigated in supramolecular chemistry as ion receptors[35,36] and, more recently, as organocatalysts.[37] Interestingly, squaramides have also been used in chemical biology, primarily in bioconjugation applications.[38] Carbohydrate conjugations mediated by squaramide tethers are often used for the grafting of carbohydrate epitopes onto peptides and proteins.[39] Some examples have been reported by Lindhorst and co-workers where heteromeric mannosides,[40] monoamides[41] and dendrimers,[42] designed as inhibitors of *E. coli* adhesin FimH, have been constructed through couplings with diethyl squarate. With these, there are very limited examples in which squaramides have been used as scaffolds to display carbohydrates in a multivalent fashion.[43]

Given the planar, aromatic character of squaramide derivatives, we synthesized a series of analogues of lead compound **1** featuring this core as a relevant comparison to the benzene glycoconjugates described in our earlier work. Diethyl squarate was reacted with propargylamine to give *N*,*N*-dipropargyl squaramide **7** (ref. 44) in 81% yield. The

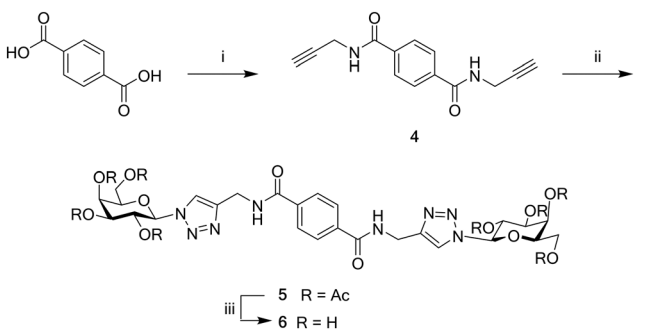

Scheme 1 Synthesis of 1,4-benzene core divalent galactosyl **6**. Reagents and conditions: i) DMTMM, propargylamine, DMF, N_2, 16 h, 81%; ii) 2,3,4,6-tetra-*O*-acetyl-1-β-azido-D-galactopyranoside,[34] $CuSO_4{\cdot}H_2O$/Na Asc, CH_3CN/H_2O, 100 °C, μw, 10 min, 73%; iii) methanol, NEt_3, H_2O, 45 °C, 6 h, 94%.

CuAAC reaction with (a) 2,3,4,6-tetra-*O*-acetyl-1-β-azido-D-galactopyranoside,[34] (b) tetra-*O*-acetyl-1-β-*O*-2-azidoethyl-D-galactopyranosyide[45] and (c) 4-*O*-(2,3,4,6-tetra-*O*-acetyl-β-D-galactopyranosyl)-2,3,6-tri-*O*-acetyl-1-β-azido-D-glucopyranoside[46] produced divalent compounds **8**,[44] **10** and **12**, respectively. Acetyl protecting groups were removed under mild basic conditions to afford **9**,[44] **11** and **13**, all of which display terminal galactosides (Scheme 2).

Norbornene derivatives have been commonly used as monomers in block copolymerization reactions[47,48] and to provide molecular frameworks for self-assembled constructs[49,50] and ion receptors.[51] Recently, in the field of peptidomimetics, a series of norbornane-based guanidines were shown to possess potent antibacterial activity[52] but there are no reports so far on these class of compounds as small molecule anti-adhesion glycoconjugates. 5-Norbornene dicarboxylic acids were then selected as suitable non-aromatic, C(sp^3) rich bicyclic aliphatic scaffolds to synthesise the next family of analogues of lead compound **1**. The use of (±) 2-*endo*-3-*exo*-dicarboxylic acid **14** (*trans*) or *endo*-2,3-dicarboxylic acid (*cis*) **18** allows for a different spatial presentation of the galactosyl moieties. In addition, while the 1,4-disubstituted and *N*,*N*-dipropargyl squaramide scaffolds described above are readily prepared, no further functionalization is possible once the grafting of the carbohydrate moieties takes place. This drawback is overcome in the norbornene derivatives, which allow for the introduction of reporter tags, such as fluorescent labels, making these analogues highly versatile.

The synthesis of the analogues of lead compound **1** based on 5-norbornene scaffolds is shown in Scheme 3. Both 5-norbornene-2-*endo*-3-*exo*-dicarboxylic acid (*trans*) **14** and the *cis*-5-norbornene-*endo*-2,3-dicarboxylic acid **18** were reacted with propargylamine and TBTU to give diamides **15** and **19**. The CuAAC reaction of **15** and **19** with 2,3,4,6-tetra-*O*-acetyl-1-β-azido-D-galactopyranoside,[34] produced the peracetylated divalent galactosides **16** (*trans*-product) and **20** (*cis*-product), respectively. Removal of the acetyl protecting groups to give final products **17** and **21** was attempted by reaction of compounds **16** and **20** under mild basic conditions. As part of the purification of the deprotected glycoconjugates, the reaction crude is generally treated with Amberlite H^+ resin. Interestingly, when this procedure was applied in the deprotection of the acetylated *cis*-norbornene **20**, treatment with the acidic resin resulted in cyclisation to the imide, loss of one of the galactosyl–triazolyl moieties and ultimately

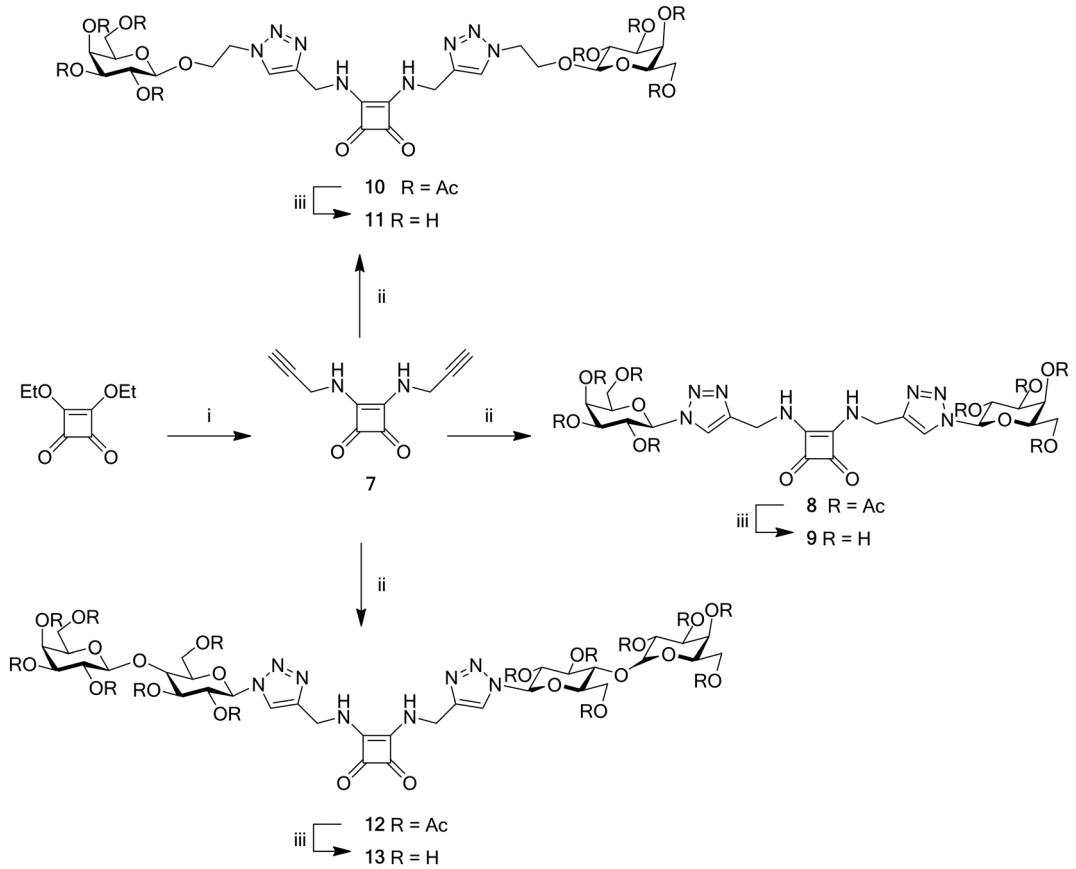

Scheme 2 Synthesis of divalent galactosyl squaramides **9**, **11** and **13**. Reagents and conditions: i) propargylamine, DMF, N_2, 16 h, 81%; ii) $CuSO_4{\cdot}5H_2O$/Na Asc, CH_3CN/H_2O, 100 °C, μW, 10 min, and a) 2,3,4,6-tetra-*O*-acetyl-1-β-azido-D-galactopyranoside,[34] 81% for **8**; (b) tetra-*O*-acetyl-1-β-*O*-2-azidoethyl-D-galactopyranosyide,[45] 80% for **9**; and (c) 4-*O*-(2,3,4,6-tetra-*O*-acetyl-β-D-galactopyranosyl)-2,3,6-tri-*O*-acetyl-1-β-azido-D-glucopyranoside,[46] 75% for **10**; iii) methanol, NEt_3, H_2O, 45 °C, 6 h, 77–99%.

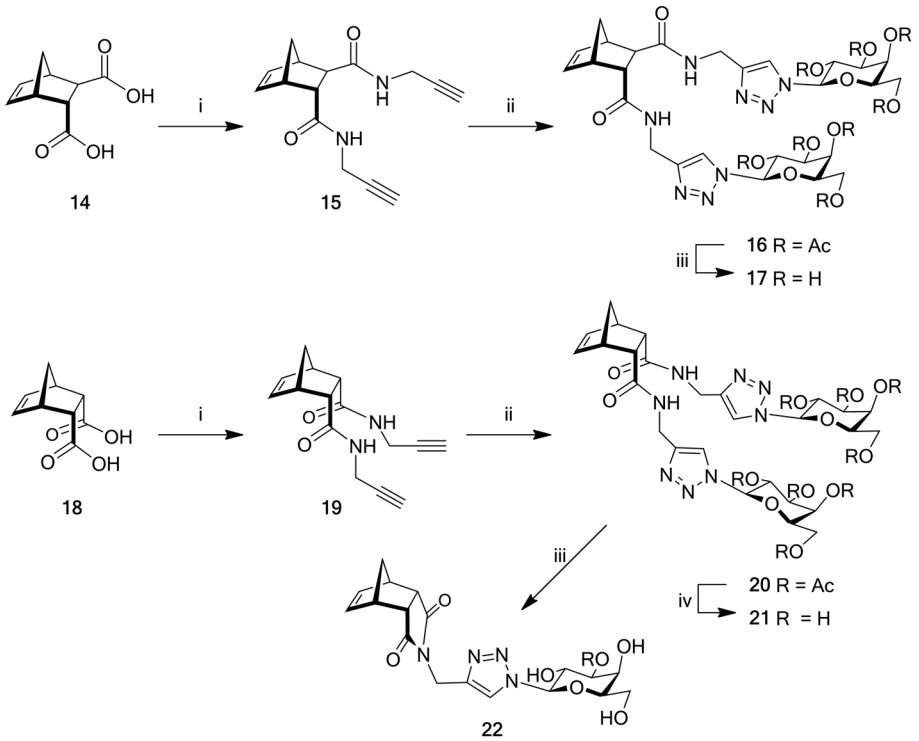

Scheme 3 Synthesis of divalent and monovalent galactosyl norbornenes **17**, **21** and **22**. Reagents and conditions: i) propargylamine, TBTU, NEt_3, DMF, N_2, 48 h, 93% for **15**, 79% for **19**; ii) 2,3,4,6-tetra-*O*-acetyl-1-β-azido-D-galactopyranoside,[34] $CuSO_4{\cdot}5H_2O$/Na Asc, CH_3CN/H_2O, 100 °C, μw, 20 min, 54% for **16**, 74% for **20**; iii) methanol, NEt_3, H_2O, 45 °C, 16 h, Amberlite H^+ resin, 30 min, 97% for **17**, quantitative yield for **22**; iv) methanol, NEt_3, H_2O, 45 °C, 16 h, 96%.

formation of the monovalent glycoconjugate **22** in quantitative yield. This unexpected reaction was not observed for the deprotection of the *trans*-compound **16**. In order to circumvent this problem, the reaction was repeated without using the resin and the desired product was isolated in 96% yield.

Biological evaluation

The adherence assays for all "second generation" compounds were carried out at a range of concentrations, using original lead compound **1** as a positive control. Toxicity assays confirmed that all compounds tested are non-toxic to *C. albicans* at the concentrations used in the adherence assays (Fig. S1†). Exclusion, competition and displacement assays (see Experimental section) were also carried out using the second generation glycoconjugates.

Firstly, an exclusion assay where the yeast cells were pre-treated with the glycoconjugates **1** and **6**, was carried out. Compound **1** (at 10 mg mL^{-1}, 13.8 mM) induced a 42% reduction in adherence, while compound **6** (at 9 mg mL^{-1}, 13.8 mM) decreased adherence by 33.5% (Fig. 2a). This assay was then performed at lower concentrations of compound **6** (1.38 mM and 138 μM). Interestingly, it was found that at lower concentrations of compound **6** there was up to a 61% reduction in adherence (Fig. 2b).

The competition assay, where yeast, BECs and glycoconjugates were co-incubated, showed a similar trend as the previous assay: compound **6** was not as efficient at reducing yeast adherence as original lead compound **1**. The competition assay was carried out again at decreasing glycoconjugate concentrations (13.8 mM, 1.38 mM and 138 μM). The average percentage decrease in adhesion is shown in Fig. 2c. As observed in the exclusion assay discussed above, the greatest anti-adhesive properties were observed at 1.38 mM.

The displacement assay, in which the yeast and BECs are co-incubated first to allow for adherence to occur, followed by subsequent addition of the glycoconjugates, provides a closer resemblance to the initial steps of *C. albicans* infection and can give useful insights into a possible therapeutic application of these compounds. Two control measurements are carried out in this experiment: control 1 involved the assessment of the binding of *C. albicans* to BECs prior to exposure to the glycoconjugates, with PBS as the control. Control 2 shows the average number of yeast attached per BEC after the second filtration of the procedure and provides an indication of physical detachment of the yeast cells, rather than inhibition of adhesion induced by the glycoconjugates. In this assay, compound **6** performed better than original compound **1**: the data identified a 56% reduction in adherence for **1** at 138 μM (compared to control 1) and a 36% reduction (compared to control 2, Fig. S2†) while compound **6** induced a 63% reduction in yeast adherence (compared to control 1) and a 48% reduction (compared to control 2, Fig. 2d).

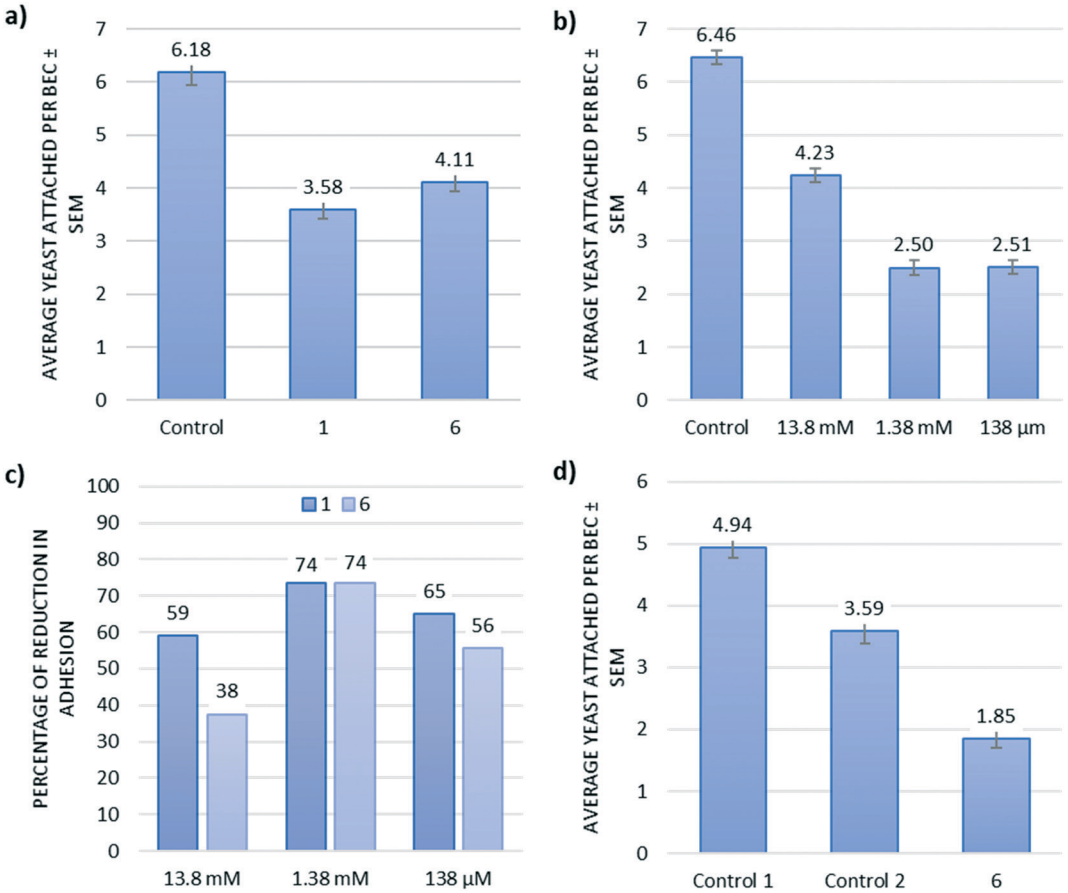

Fig. 2 Anti-adherence evaluation of glycoconjugate **6** with a 1,4-aromatic core: a) exclusion assay showing average number of yeast attached per BEC ([glycoconjugates] = 13.8 mM), control: phosphate buffer solution (PBS); b) exclusion assay showing average number of yeast attached per BEC at [**6**], control: PBS; c) competitive assay showing the percentage decrease in adhesion induced by glycoconjugates **1** and **6**; d) displacement assay showing the average number of yeast attached per BEC for glycoconjugate **6** at [138 µM], control 1: PBS, control 2: average number of yeast attached per BEC treated with control 1 after the second filtration (provides an indication of physical detachment of the yeast cells).

The squaramide glycoconjugates **9**, **11** and **13** did not display better anti-adhesive properties than the original lead compound **1** in exclusion assays. While compound **1** was capable of reducing yeast adherence by 45%, squaramides **11** and **13** showed similar results, reducing adherence by 33–34%. Compound **9**, which structurally only differs to lead compound **1** in the 4-membered cyclic core, did not perform as well as the other squaramides, producing only a 27% reduction in adhesion (Fig. 3a). If the exclusion assay is performed in reverse (with BECs pre-treated with the glycoconjugates prior to exposure to the yeast), the percentage reduction decreases for all compounds tested (Fig. 3b). This may indicate that the glycoconjugates interact more favourably with structural elements in *C. albicans* than in the BECs. In the competitive assay, compound **1** again showed the best results, inhibiting adhesion by 41%. Compounds **11** and **13** showed similar performance, inhibiting adhesion by 31–36%. Compound **9** again produced the lowest decrease in adhesion, only 17%. (Fig. 3c). The displacement assay was performed on the two best-performing squaramides **11** and **13**. Compounds **11** and **13** at [glycoconjugates] = 13.8 mM produced a reduction of yeast adhesion of 35% and 39% respectively (compared to control 1) and 21 and 25% reduction, respectively (compared to control 2, Fig. 3d). The displacement assay of original lead compound **1** at 13.8 mM showed slightly higher anti-adhesive properties, with a reduction of yeast adherence of 42% (compared to control 1) and 31% (compared to control 2, Fig. S3†). These results indicate that divalent terminal galactosides with a benzene-aromatic core seem to be more efficient inhibitors of *C. albicans* adhesion to BECs than their counterparts built on aromatic-squaramide scaffolds.

The norbornene derivatives **17**, **21** and **22** were similarly evaluated in a range of anti-adhesion assays. In the exclusion assay (Fig. 4a) where the yeast was pre-treated, the glycoconjugates were compared to lead compound **1**, which reduced adherence by 51% in this particular assay. The *cis*-norbornene compound **21** showed very promising results in this assay with a 65% inhibition of adherence of the yeast to the BECs, performing better than lead compound **1**. The *trans*-norbornene compound **17** and the monovalent derivative **22** showed similar results to the original lead **1**, reducing yeast adherence by 46% and 43%, respectively In the competition assay (Fig. 4b), the two divalent galactosyl norbornenes **17** and

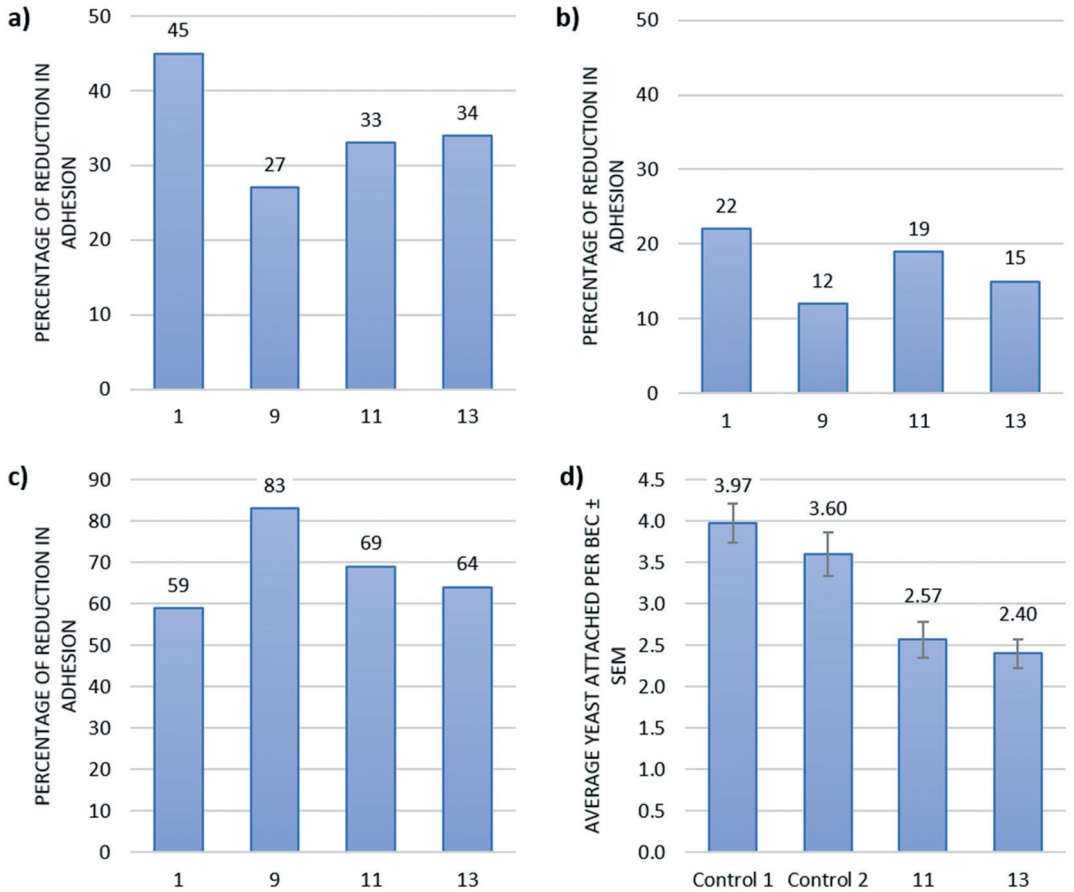

Fig. 3 Anti-adherence evaluation of glycoconjugates **9**, **11** and **13** with squaramide core: exclusion assay where a) the yeast are pre-treated and b) the BEC are pre-treated; c) competitive assay showing the percentage decrease in adhesion induced by the glycoconjugates; d) displacement assay showing the average number of yeast attached per BEC for glycoconjugates **11** and **13**, control 1: PBS, control 2: average number of yeast attached per BEC treated with control 1 after the second filtration (provides an indication of physical detachment of the yeast cells). All compounds were tested at 13.8 mM.

21 showed similar results, causing a greater reduction of yeast adherence than the lead compound **1**. The monovalent derivative **22** did not have a significant effect on yeast adhesion (17% inhibition). Finally, the displacement assay (Fig. 4c) showed that the divalent *trans*-norbornene **17** and the monovalent compound **22** show again very similar results, with a 23% reduction in adherence compared to control 1, and only 7–8% reduction compared to control 2. On the other hand, the divalent *cis*-norbornene compound **21** presented the best results with 45% reduction in adherence compared to control **1**, and 34% reduction compared to control 2, again outperforming lead compound **1** (42% and 31% inhibition at [**1**] = 13.8 mM, compared to control **1** and **2**, respectively, as outlined earlier, Fig. S3†). These results highlight the important role of the preorganised configurations that are enabled by the norbornene scaffolds, with a remarkable difference in activity between the *trans* and *cis* glycoconjugates **17** and **21**.

Conformational analysis

In order to explore the conformational space accessible to compounds **1** and **21**, a detailed geometric and conformational analysis was performed on both systems employing both semi-empirical molecular dynamics (MD) simulations and high-level quantum chemistry calculations (Fig. S4–S8†). Initial pre-screening of the conformational space was achieved by means of the conformer-rotamer ensemble sampling tool (crest) that utilizes the GFN2-xTB method. The method is designed around a semiempirical tight-binding quantum model to facilitate efficient and robust screening of the conformational space of large molecular systems. This procedure runs through iterative metadynamics sampling and subsequent optimizations steps of selected MTD snapshots, narrowing down the number of reasonable conformers for compound **1** and **21**, respectively. These final structures were then subjected to more accurate density functional theory (DFT) geometry optimisations, which allowed for their ranking in terms of their relative enthalpies (Tables S1 and S2†). These results pointed towards a relatively large number of conformers for **1** within a 10 kcal mol^{-1} bracket of the lowest energy conformer. A common structural feature of these conformers is the presence of intramolecular hydrogen bonds, involving the OH groups of the terminal galactosyl units, triazolyl, amide carbonyl and

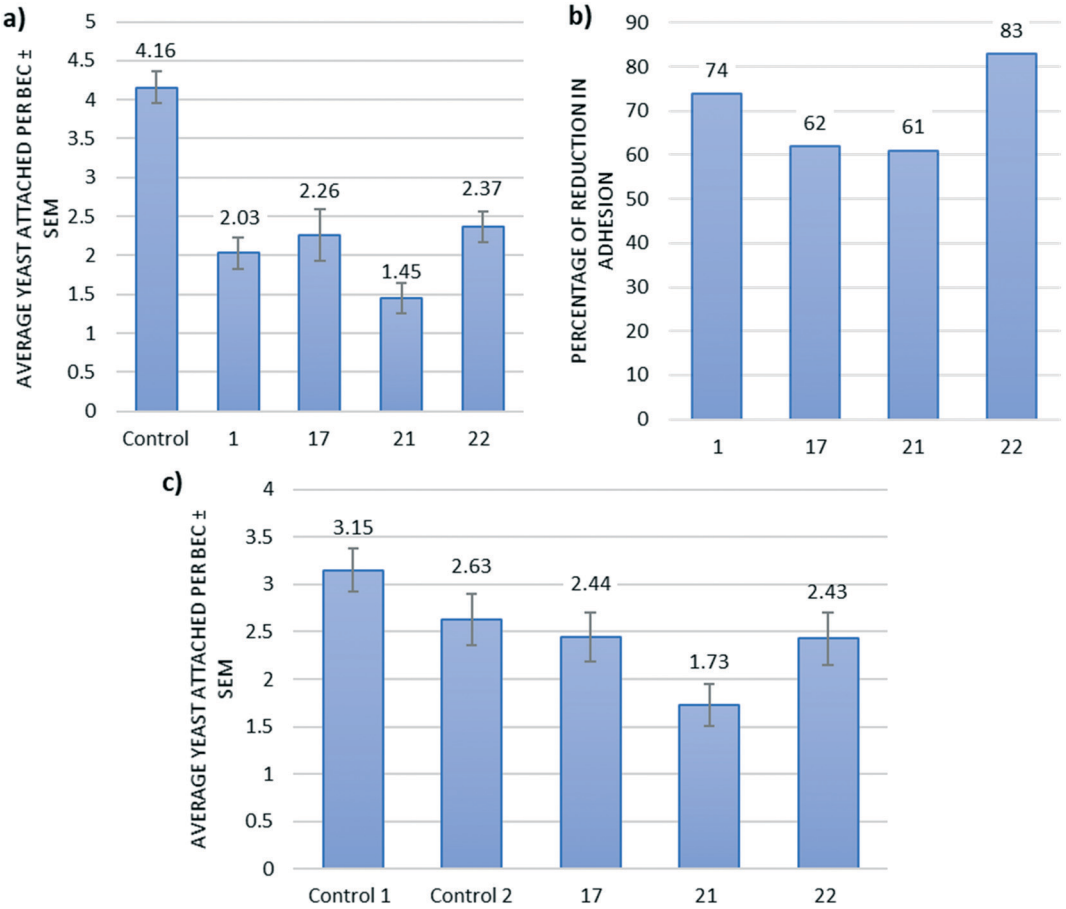

Fig. 4 Anti-adherence evaluation of glycoconjugates **17**, **21** and **22** with a norbornene core: a) exclusion assay showing average number of yeast attached per BEC, control: PBS; b) competition assay showing the percentage decrease in adhesion of *C. albicans* to BECs, control: PBS; c) displacement assay showing the average number of yeast attached per BEC, control 1: PBS, control 2: average number of yeast attached per BEC treated with control 1 after the second filtration (provides an indication of physical detachment of the yeast cells). All compounds were tested at 13.8 mM.

NH groups. These contacts give rise to more or less globular and "semi-open" structural motifs within the various conformers. Two representative examples of this stabilisation are shown in Fig. 5. Considering all low energy conformers, from this analysis the distances between the anomeric carbon centres are typically in the range 6–15 Å. A maximally elongated but highly destabilised conformer gives an estimate of the longest possible distance of 18 Å. There are no obvious hydrophobic interactions involving apolar C–H from the galactoses and the aromatic ring in the molecule. In comparison, the *cis*-norbornene core in **21** encourages the formation of basket-shaped conformers, which are stabilised *via* internal hydrogen bonding between the galactosyl and triazolyl residues of adjacent branches. The distances between the anomeric centres in these conformers fall into the range 4–6 Å, distinctly shorter than for **1**. In contrast, in an open conformer in which both sugar residues are placed approximately furthest apart, gives a separation of the anomeric centres of ~15 Å.

Further insight into the dynamical behaviour of **1** and **21** was obtained from MD simulations performed on these two molecules, employing both implicit and explicit solvation models. One protocol utilized well-tempered metadynamics simulations in a GBSA continuum to crudely account for the presence of water as solvent, defining two collective variables (CV) as the torsional angles of the amide bonds connecting the side-arms to the core scaffold (Fig. 6). Analysis of the combined trajectories for both **1** (Fig. S9†) and **21** (Fig. S10†) resulting from these simulations reveals that the characteristic distances between anomeric centres fall into the ranges 10–18 Å and 4–10 Å for or **1** and **21**, respectively. These values are in good agreement with the results from the initial survey of the conformational space described above. Plots of the accessible conformational space are shown in Fig. S11.† It is interesting to note that the free energy surface (FES) for compound **21** is smoother, pointing to a larger number of low-energy conformers. This can be rationalised with the fact that both linkers are attached from the same *endo* side to the bicyclic core. Their spatial proximity enables stabilisation of conformers through strong hydrogen-bonding between the OH groups of the sugars, CONH and triazolyl groups of adjacent arms. This preference of a closed basket-like structure for compound **21** is

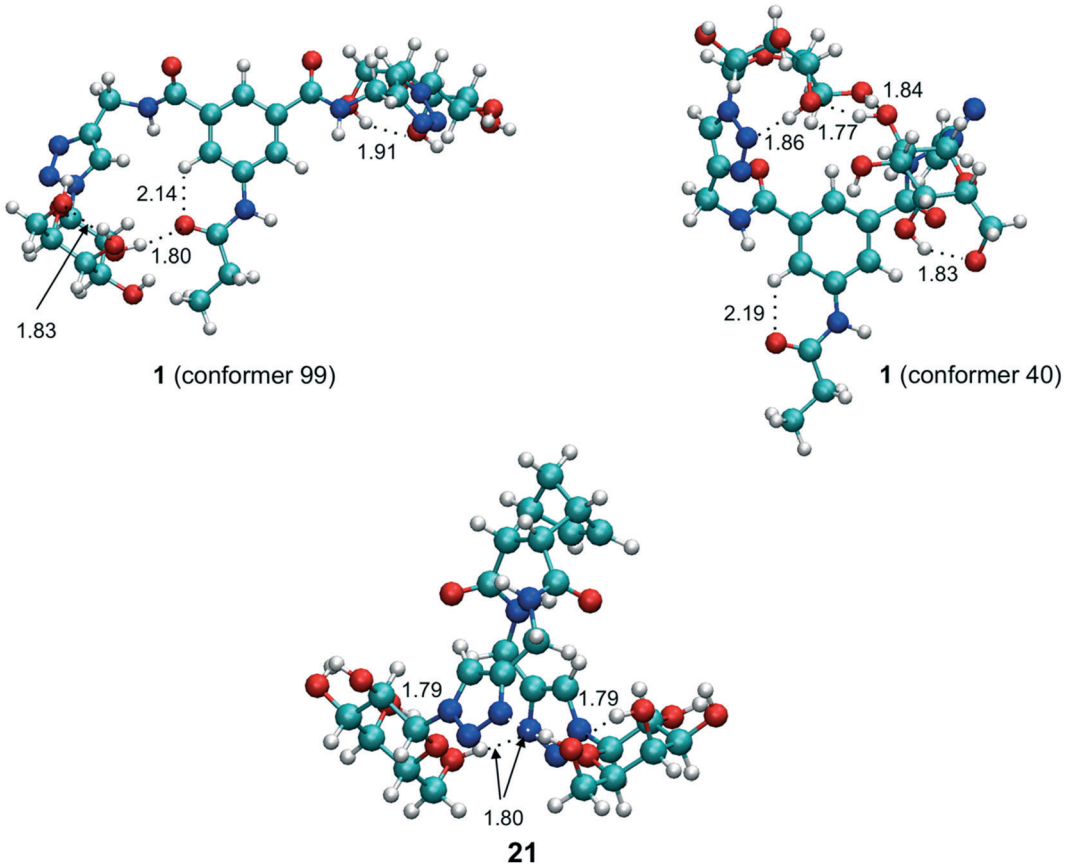

Fig. 5 Geometries (SMD-B3PW91/6-31G**) of selected low-energy conformers of compounds **1** and **21** along with selected hydrogen-bond distances (given in Å). Oxygens red, nitrogen blue, carbon cyan, hydrogen white.

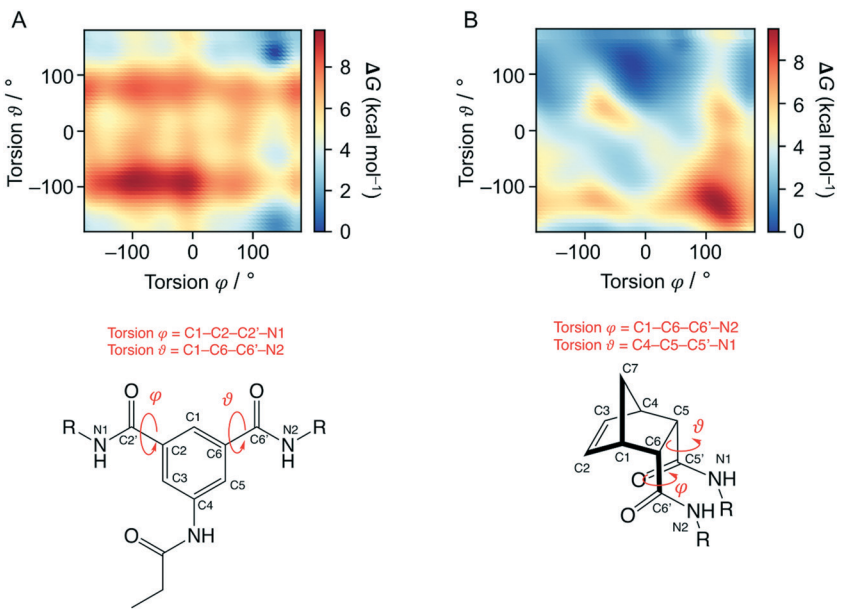

Fig. 6 Plots of the free energy surface (FES) and definition of the torsional angles used as collective variables (CV) for compound **1** (A) and compound **21** (B).

also reflected in the molecular dynamics simulations invoking explicit solvent water molecules. A "closed" and "open" structure obtained from a snapshot of the above metadynamics simulations was taken as starting point for these "water droplet"

simulations carried out at the QM/MM level of theory (Fig. S12–14†). The closed form largely maintains its basked-shaped structure, with the distance between the anomeric centres fluctuating around ~5.5 Å, whilst the open form with galactosyl units initially further apart eventually converges back towards a closed form (Fig. S15†). Whilst the conformational analysis of the above compounds predicts a diverse range of orientations of the terminal sugar residues, it is important to note that more extended conformers may still be important when the ligand binds to the target protein. It has been demonstrated that flexible drug molecules adopt more compact forms in the homogenous bulk solvent environment,[52] but binding to anisotropic receptor binding sites can often induce unfolding to open conformer forms. In the absence of structural information of the target binding site of the protein, structural proposals of the binding conformer are unattainable.

Conclusion

In summary, the molecular scaffold is a critical structural element in the design of anti-adhesion glycoconjugates. Adherence to host tissue is essential for the fungal pathogen *C. albicans* to colonise and disseminate through the host. The ability to inhibit adherence or to reverse this process offers a novel therapeutic approach for the treatment of *Candida* infections of the mucosal surfaces. A series of divalent galactosides built on aromatic (benzene, squaramide) and bicyclic aliphatic (norbornene) molecular scaffolds have been synthesised and their activities as inhibitors of the adhesion of fungal pathogen *C. albicans* have been evaluated. The results show that the glycoconjugates featuring a benzene core (*i.e.* lead compound **1** and 1,4-disubstitued aromatic compound **6**) performed significantly better than the squaramide analogues. On the other hand, divalent galactosides based on norbornene scaffolds display anti-adhesive properties comparable to lead compound **1**, with *cis*-norbornene derivative **21** slightly outperforming it in some assays. Conformational analysis reveals compound **1** to be significantly more flexible than **21**, but both molecules show a preference for folded conformations, which leaves the distance between anomeric centres in the ranges of 10–18 Å and 4–10 Å for **1** and **21**, respectively, in the lowest energy conformers. In the absence of structural knowledge of the target carbohydrate-binding protein mediating adhesion in *C. albicans*, the structure–activity relationship study and conformational analysis described in this work provide valuable data for the development of inhibitors of fungal adhesion. Saturated bicyclic scaffolds are emerging alternatives to phenyl derivatives in the discovery of bioactive molecules. The compounds reported in this study are, to the best of our knowledge, the first example of small molecule anti-adhesion glycoconjugates built on norbornene scaffolds. The results from this study highlight the potential of underexplored molecular scaffolds, such as norbornenes, in the design and synthesis of glycomimetics and multivalent glycoconjugates.

Experimental section

Chemistry synthesis

General methods. All reagents for synthesis were bought commercially and used without further purification. Dichloromethane (DCM) was freshly distilled over CaH_2 prior to use. Reactions were monitored with thin layer chromatography (TLC) on Merck silica gel F_{254} plates. Detection was effected by UV (λ = 254 nm) or charring in a mixture of 5% sulfuric acid–ethanol. NMR spectra were recorded using Bruker Ascend 500 spectrometer at 293 K. All chemical shifts were referenced relative to the relevant deuterated solvent residual peaks. Assignments of the NMR spectra were deduced using ^{1}H NMR and ^{13}C NMR, along with 2D experiments (COSY, HSQC and HMBC). Chemical shifts are reported in ppm. Flash chromatography was performed with Merck silica gel 60. Microwave reactions were carried out using a CEM Discover microwave synthesizer. Optical rotations were obtained from an AA-100 polarimeter and $[\alpha]_D$ values are given in 10^{-1} cm^2 g^{-1}. High performance liquid chromatography analysis (HPLC, Waters Alliance 2695) was performed in final compounds and indicated purity of 95% based on integrations without the use of an internal standard. High resolution mass spectrometry (HRMS) was performed on an Agilent-LC 1200 series coupled to a 6210 Agilent time-of-flight (TOF) mass spectrometer equipped with an electrospray source in both positive and negative (ESI+/−) modes. Infrared spectra were obtained *via* ATR as a solid on a zinc selenide crystal or as a film on NaCl plates in the region 4000–400 cm^{-1} on a Perkin Elmer Spectrum 100 FT-IR spectrophotometer. Spectroscopic data for all compounds are provided in the ESI.†

General copper-catalyzed azide–alkyne cycloaddition (CuAAC) reaction procedures. Copper sulphate pentahydrate (20 mg) and sodium ascorbate (40 mg) were added to a solution of the acetylated sugar azide (1.25 equiv per propargyl group) and the corresponding propargyl amide scaffold in acetonitrile/water (2 : 1 ratio). The reaction was heated (μw at 100 °C) with stirring until deemed complete by TLC analysis (typically 5–15 min). The solvent was removed *in vacuo*. The residue was dissolved in DCM, washed with water (×3) and dried ($MgSO_4$). The mixture was filtered and the solvent was removed *in vacuo* to yield the crude product, which was purified by silica gel column chromatography (DCM : MeOH 98 : 2–93 : 7) to give the corresponding product.

General acetyl ester hydrolysis procedure. The acetylated glycoconjugate was dissolved in methanol/water (2 : 1 ratio). NEt_3 (0.1 mL) was added and the reaction mixture was allowed to stir at 45 °C until completion (typically 6–18 h). The solution was cooled to rt, Amberlite H^+ was added and the mixture was allowed to stir for 30 min. The solution was filtered and the solvent was removed in the rotatory evaporator and the residue was dried under high vacuum or lyophilized to give the deprotected glycoconjugate.

N,N′-di-(2,3,4,6-tetra-O-acetyl-β-D-galactopyranosyl-1,2,3-triazol-4-ylmethyl)-terephthalamide (5)

Prepared from **4** (ref. 33) and 2,3,4,6-tetra-*O*-acetyl-1-β-azido-D-galactopyranoside,[34] according to general CuAAC procedure. Off-white amorphous solid (164 mg, 73%). R_f = 0.36 (DCM : MeOH 9 : 1). $[\alpha]_D^{24}$: −10.9° (*c* 1.1, DCM). ^{1}H NMR (500 MHz, $CDCl_3$) δ 7.95 (s, 2H, triaz-H), 7.83 (s, 4H, Ar–H), 7.34–7.27 (m, 2H, N*H*CH$_2$-triaz), 5.85 (d, *J* = 9.3 Hz, 2H, H-1), 5.58–5.51 (m, 4H, H-2 and H-4), 5.27 (dd, *J* = 10.3, 3.4 Hz, 2H, H-3), 4.82–4.64 (m, 4H, C*H*$_2$-triaz), 4.28–4.23 (m, 2H, H-5), 4.17 (ddd, *J* = 18.3, 11.4, 6.4 Hz, 4H, H-6 and H-6′), 2.22 (s, 6H, OAc), 2.03 (s, 6H, OAc), 2.01 (s, 6H, OAc), 1.86 (s, 6H, OAc). ^{13}C NMR (126 MHz, $CDCl_3$) δ 170.3 (CO of OAc), 170.0 (CO of OAc), 169.8 (CO of OAc), 169.0 (CO of OAc), 166.6 (*C*ONH), 145.1 (CH$_2$*C*CH), 136.7 (Ar–C), 127.4 (Ar–*C*H), 121.3 (CH$_2$C*C*H), 86.3 (C-1), 74.1 (C-5), 70.7 (C-3), 68.1 (C-2/C-4), 66.8 (C-2/C-4), 61.2 (C-6), 35.4 (*C*H$_2$-CCH), 20.7 (CH$_3$ of OAc), 20.6 (CH$_3$ of OAc), 20.5 (CH$_3$ of OAc), 20.2 (CH$_3$ of OAc). IR (ATR): 3380, 1743, 1644, 1533, 1495, 1431, 1368, 1212, 1046, 923 cm^{-1}. HRMS (ESI+): *m*/*z* calculated for $C_{42}H_{50}N_8O_{20}$ + Na^+ [M + Na^+]: 1009.3039. Found 1009.3032.

N,N′-di-(β-D-galactopyranosyl-1,2,3-triazol-4-ylmethyl)-terephthalamide (6)

Prepared from **5** according to general acetyl ester hydrolysis procedure. White amorphous solid (59 mg, 90%). $[\alpha]_D^{23}$: 13.75° (*c* = 0.8, H_2O). ^{1}H NMR (500 MHz, D_2O) δ 8.15 (s, 2H, triaz-H), 7.54 (s, 4H, Ar–H), 5.56 (d, *J* = 9.2 Hz, 2H, H-1), 4.47 (s, 4H, C*H*$_2$-triaz), 4.11 (t, *J* = 9.5 Hz, 2H, H-2), 3.96 (d, *J* = 3.2 Hz, 2H, H-4), 3.85 (t, *J* = 6.1 Hz, 2H, H-5), 3.76 (dd, *J* = 9.8, 3.3 Hz, 2H, H-3), 3.64 (d, *J* = 6.2 Hz, 4H, H-6 and H-6′). ^{13}C NMR (125 MHz, D_2O) δ 168.9 (CO), 144.6 (CH$_2$*C*CH), 135.9 (Ar–C), 127.4 (Ar–*C*H), 123.2 (CH$_2$C*C*H), 88.2 (C-1), 78.3 (C-5), 72.9 (C-3), 69.8 (C-2), 68.6 (C-4), 60.9 (C-6), 34.8 (*C*H$_2$CCH). IR (NaCl disc): 3290, 1636, 1542, 1498, 1293, 1091, 1053, 890 cm^{-1}. HRMS (ESI+): *m*/*z* calculated for $C_{26}H_{34}N_8O_{12}$ + Na^+ [M + Na^+]: 673.2194. Found 673.2206.

3,4-di(2-O-(2,3,4,6-tetra-O-acetyl-β-D-galactopyranosyl)-ethyl-1,2,3-triazol-4-ylmethylamino)cyclobut-3-ene-1,2-dione (10)

Prepared from **7** (ref. 44) and 2-*O*-(2,3,4,6-tetra-*O*-acetyl-β-D-galactopyranosyl)ethyl azide[45] according to general CuAAC procedure. Yellow amorphous solid (197 mg, 80%). R_f = 0.5 (DCM : MeOH 9 : 1). $[\alpha]_D^{22}$: −3.8° (*c* = 1.05, DCM). ^{1}H NMR (500 MHz, $CDCl_3$) δ 8.06 (s, 2H, N*H*CH$_2$-triaz), 7.78 (s, 2H, triaz-H), 5.38 (d, *J* = 3.4 Hz, 2H, H-4), 5.15 (dd, *J* = 10.4, 8.0 Hz, 2H, H-2), 5.04–4.86 (m, 6H, H-3 and C*H*$_2$CCH), 4.68–4.53 (m, 4H, C*H*$_2$CH$_2$O), 4.51 (d, *J* = 7.9 Hz, 2H, H-1), 4.25–4.18 (m, 2H, C*H*O-Gal), 4.11 (ddd, *J* = 30.2, 11.3, 6.7 Hz, 4H, H-6 and H-6′), 4.02–3.94 (m, 2H, C*H*O-Gal), 3.92 (t, *J* = 6.6 Hz, 2H, H-5), 2.17 (s, 6H, OAc), 2.04 (s, 6H, OAc), 1.98 (s, 6H, OAc), 1.96 (s, 6H, OAc). ^{13}C NMR (126 MHz, $CDCl_3$) δ 183.6 (CO), 170.4 (CO of OAc), 170.2 (CO of OAc), 170.1 (CO of OAc), 169.4 (CO of OAc), 167.7 (NH*C*CO), 144.7 (CH$_2$*C*CH), 124.4 (CH$_2$C*C*H), 100.9 (C-1), 70.9 (C-5), 70.6 (C-3), 68.5 (C-2), 67.3 (CH$_2$*C*H$_2$O), 66.9 (C-4), 61.1 (C-6), 50.3 (*C*H$_2$CH$_2$O), 38.6 (*C*H$_2$CCH), 20.7 (CH$_3$ of OAc), 20.7 (CH$_3$ of OAc), 20.5 (CH$_3$ of OAc). IR (NaCl disc): 3261, 2964, 1750, 1677, 1602, 1535, 1432, 1370, 1227, 1175, 1139, 1059 cm^{-1}. HRMS (ESI+): *m*/*z* calculated for $C_{42}H_{54}N_8O_{22}$ + Na^+ [M + Na^+]: 1045.3250. Found 1045.3249.

3,4-di(2-O-(β-D-galactopyranosyl)-ethyl-1,2,3-triazol-4-ylmethylamino)cyclobut-3-ene-1,2-dione (11)

Prepared from **10** according to general acetyl ester hydrolysis procedure. White amorphous solid (95 mg, 94%). $[\alpha]_D^{22}$: 12.0° (*c* = 1, H_2O). ^{1}H NMR (500 MHz, D_2O) δ 8.01 (s, 2H, triaz-H), 4.85 (s, 4H, C*H*$_2$CCH), 4.62 (t, *J* = 5.0 Hz, 4H, O–CH$_2$C*H*$_2$), 4.27 (d, *J* = 7.9 Hz, 2H, H-1), 4.25–4.20 (m, 2H, O–C*H*–CH$_2$), 4.09–4.02 (m, 2H, O–C*H*–CH$_2$), 3.84 (d, *J* = 3.4 Hz, 2H, H-4), 3.70–3.63 (m, 4H, H-6 and H-6′), 3.59 (dd, *J* = 7.4, 4.8 Hz, 2H, H-5), 3.54 (dd, *J* = 9.9, 3.5 Hz, 2H, H-3), 3.41 (dd, *J* = 9.9, 7.9 Hz, 2H, H-2). ^{13}C NMR (125 MHz, D_2O) δ 182.22 (CO), 168.0 (*C*CO), 144.5 (CH$_2$*C*CH), 124.70 (CH$_2$C*C*H), 102.95 (C-1), 75.07 (C-5), 72.54 (C-3), 70.51 (C-2), 68.48 (C-4), 67.95 (O–*C*H$_2$CH$_2$), 60.85 (C-6), 50.38 (O–CH$_2$*C*H$_2$), 38.82 (*C*H$_2$CCH). IR (ATR): 3269, 2924, 1800, 1662, 1591, 1531, 1427, 1338, 1224, 1140, 1042, 889, 826, 775 cm^{-1}. HRMS (ESI+): *m*/*z* calculated for $C_{26}H_{38}N_8O_{14}$ + H^+ [M + H^+]: 686.2586. Found 687.2576.

3,4-di-[{4-O-(2,3,4,6-tetra-O-acetyl-β-D-galactopyranosyl)-2,3,6-tri-O-acetyl-β-D-glucopyranosyl}-1,2,3-triazol-4-ylmethylamino]cyclobut-3-ene-1,2-dione (12)

Prepared from **7** (ref. 44) and 4-*O*-(2,3,4,6-tetra-*O*-acetyl-β-D-galactopyranosyl)-2,3,6-tri-*O*-acetyl-1-β-azido-D-glucopyranoside[46] according to general CuAAC procedure. White amorphous solid (529 mg, 75%). R_f = 0.27 (DCM : MeOH 9 : 1). $[\alpha]_D^{24}$: 7.0° (*c* = 1.0, DCM). ^{1}H NMR (500 MHz, $CDCl_3$) δ 8.23 (s, 2H, N*H*CH$_2$-triaz), 8.09 (s, 2H, triaz-H), 6.07 (d, *J* = 6.4 Hz, 2H, H-1 Gal), 5.49–5.38 (m, 4H, H-2 Gal and H-3 Gal), 5.36 (d, *J* = 3.3 Hz, 2H, H-4 Glc), 5.11 (dd, *J* = 10.2, 8.0 Hz, 2H, H-2 Glc), 4.99 (dd, *J* = 10.4, 3.3 Hz, 2H, H-3 Glc), 4.94 (apps, 4H, C*H*$_2$-triaz), 4.58 (d, *J* = 7.9 Hz, 2H, H-1 Glc), 4.51 (d, *J* = 11.6 Hz, 2H, H-6 Glc), 4.28–4.05 (m, 10H, H-6′ Glc, H-5 Gal, H-4 Gal, H-6 and H-6′ Gal), 4.03–3.92 (m, 2H, H-5 Glc), 2.14 (s, 6H, OAc), 2.06 (s, 6H, OAc), 2.04 (appd, 18H, 3× OAc), 1.95 (s, 6H, OAc), 1.76 (s, 6H, OAc). ^{13}C NMR (126 MHz, $CDCl_3$) δ 183.6 (CO), 170.4 (CO of OAc), 170.2 (CO of OAc), 170.0 (CO of OAc), 169.9 (CO of OAc), 169.7 (CO of OAc), 169.2 (CO of OAc), 168.9 (CO of OAc), 167.6 (NH*C*CO), 145.1 (CH$_2$*C*CH), 123.5 (CH$_2$C*C*H), 101.2 (C-1 Glc), 85.4 (C-1 Gal), 75.9 (C-4/5 Gal), 75.6 (C-4/5 Gal), 72.6 (C-3 Gal), 71.0 (C-3 Glc), 70.8 (C-2 Gal), 70.7 (C-5 Glc), 69.1 (C-2 Glc), 66.8 (C-4 Glc), 61.9 (C-6 Glc), 60.8 (C-6 Gal), 38.4 (*C*H$_2$CCH), 20.9 (CH$_3$ of OAc), 20.8 (CH$_3$ of OAc), 20.7 (CH$_3$ of OAc), 20.6 (CH$_3$ of OAc), 20.5 (CH$_3$ of OAc), 20.3 (CH$_3$ of OAc), 20.1 (CH$_3$ of OAc). IR (NaCl disc): 3478, 3263, 2964, 1753, 1597, 1536, 1370, 1227, 1048 cm^{-1}. HRMS (ESI+): *m*/*z* calculated for $C_{62}H_{78}N_8O_{36}$ + Na^+ [M + Na^+]: 1533.4416. Found 1533.3743.

3,4-di-[{4-O-(β-D-galactopyranosyl)-β-D-glucopyranosyl}-1,2,3-triazol-4-ylmethylamino]cyclobut-3-ene-1,2-dione (13)

Prepared from **12** according to general acetyl ester hydrolysis procedure. White amorphous solid (172 mg, 99%). $[\alpha]_D^{22}$: 10°

(c = 1, H_2O). ^{1}H NMR (500 MHz, D_2O) δ 8.11 (appd, J = 3.0 Hz, 2H, triaz-H), 5.70–5.59 (m, 2H, H-1), 4.81 (s, 4H, CH_2-CCH), 4.47 (d, J = 7.9 Hz, 1H, H-1 Glc), 4.40 (d, J = 7.8 Hz, 1H, H-1 Glc), 3.99–3.42 (m, 24H). ^{13}C NMR (126 MHz, D_2O) δ 182.3 (CO), 168.2 (*C*CO), 144.9 (CH$_2$*C*CH), 123.3 (CH$_2$C*C*H), 102.9 (C-1 Glc), 96.4 (C-1 Glc), 87.5 (C-1 Gal), 78.9, 77.7, 77.4, 75.9, 75.4, 75.1, 74.5, 72.8, 72.5, 72.2, 71.9, 71.9, 70.9, 70.5, 69.2, 68.9, 68.7, 68.6, 68.3, 61.2, 61.1, 61.0, 60.4, 59.7, 38.8 (*C*H$_2$CCH). IR (ATR): 3300, 2939, 2452, 1803, 1670, 1585, 1516, 1379, 1015 cm^{-1}. HRMS (ESI+): m/z calculated for $C_{34}H_{50}N_8O_{22}$ + Na$^+$ [M + Na$^+$]: 945.2937. Found 945.2967.

Bicyclo[2.2.1]hept-5-ene-2-*endo*-3-*exo*-2,3-dicarboxamide, *N*-(prop-2-yn-1-yl) (15)

5-Norbornene-2-*endo*-3-*exo*-dicarboxylic acid **14** (200 mg, 1.098 mmol) and TBTU (881 mg, 2.7 mmol) were dissolved in anhydrous DMF (15 mL) under N_2. NEt$_3$ (0.38 mL, 2.7 mmol) and propargylamine (0.15 mL, 2.3 mmol) were added after 10 min. The reaction was allowed to stir for 48 h. DMF was removed *in vacuo*, the resulting residue was dissolved in DCM (20 mL) and washed with brine (3 × 20 mL), dried ($MgSO_4$), filtered and concentrated *in vacuo* to yield the crude product. This was then purified by silica gel column chromatography (1 : 1–1.5 : 1 EtOAc : pet. ether) to give **15**: white solid (260 mg, 93%). R_f =0.25 (1 : 1 EtOAc : pet. ether). ^{1}H NMR (500 MHz, MeOD) δ 6.29 (dd, J = 5.6, 3.1 Hz, 1H, H$_{e/f}$), 6.05 (dd, J = 5.6, 2.8 Hz, 1H, H$_{e/f}$), 4.04–3.87 (m, 4H, CH_2CCH), 3.26 (dd, J = 4.6, 3.7 Hz, 1H, H$_{b/c}$), 3.21 (d, J = 0.6 Hz, 1H, H$_{a/d}$), 2.95 (dd, J = 1.9, 1.1 Hz, 1H, H$_{a/d}$), 2.59–2.55 (m, 3H, CH$_2$CC*H* and H$_{b/c}$), 1.82 (d, J = 8.4 Hz, 1H, H$_g$), 1.41 (dq, J = 8.4, 1.7 Hz, 1H, H$_{g'}$). ^{13}C NMR (125 MHz, MeOD) δ 174.8 (CO), 173.7 (CO), 137.4 (C$_{e/f}$), 134.1 (C$_{e/f}$), 70.6 (CH$_2$-C*C*H), 70.4 (CH$_2$C*C*H), 48.5 (C$_{a/d}$), 48.1 (C$_{b/c}$), 47.1 (C$_{b/c}$), 47.0 (C$_g$), 46.1 (C$_{a/d}$), 28.3 (*C*H$_2$CCH), 28.1 (*C*H$_2$CCH), 13.1. IR (ATR): 3284, 1635, 1531, 1447, 1333, 1276, 1215, 1031, 862 cm^{-1}. HRMS (ESI+): m/z calculated for $C_{15}H_{16}N_2O_2$ + Na$^+$ [M + Na]$^+$: 279.1109. Found 279.1119.

Bicyclo[2.2.1]hept-5-ene-2-*endo*-3-*exo*-2,3-dicarboxamide, *N*-(2,3,4,6-tetra-*O*-acetyl-β-D-galactopyranosyl-1,2,3-triazol-4-ylmethyl) (16)

Prepared from **15** and 2,3,4,6-tetra-*O*-acetyl-1-β-azido-D-galactopyranoside[34] according to general CuAAC procedure. Off-white solid (488 mg, 54%). R_f =0.58 (DCM : MeOH 9 : 1). $[\alpha]_D^{23}$: −6.0° (c = 1, DCM). ^{1}H NMR (500 MHz, $CDCl_3$) δ 7.79 (d, J = 6.7 Hz, 1H, triaz-H), 7.75 (s, 1H, triaz-H′), 7.17 (dt, J = 9.0, 5.8 Hz, 1H, N*H*CH$_2$-triaz), 6.93 (dt, J = 24.9, 5.7 Hz, 1H, N*H*′CH$_2$-triaz), 6.16 (td, J = 5.7, 3.2 Hz, 1H, H$_{e/f}$), 6.08–6.02 (m, 1H, H$_{e/f}$), 5.82 (d, J = 9.2, 2H, H-1), 5.52–5.42 (m, 4H, H-2 and H-4), 5.24 (dd, J = 10.3, 3.2 Hz, 2H, H-3), 4.49–4.37 (m, 4H, CH_2-triaz ×2), 4.29–4.18 (m, 2H, H-5), 4.18–4.04 (m, 4H, H-6 and H-6′), 3.11–3.00 (m, 2H, H$_{a/d}$ and H$_{b/c}$), 2.97 (s, 1H, H$_{a/d}$), 2.40 (dd, J = 12.7, 3.7 Hz, 1H, H$_{b/c}$), 2.18–2.13 (m, 6H, OAc), 1.98–1.92 (m, 12H, OAc), 1.86–1.75 (m, 6H, OAc), 1.75–1.70 (m, 1H, H$_g$), 1.41 (d, J = 8.5 Hz, 1H, H$_{g'}$). ^{13}C NMR (126 MHz, $CDCl_3$) δ 173.7 and 173.6 (*C*O-NHCH$_2$), 172.6 and 172.5 (*C*′O–NHCH$_2$), 169.3 (CO of OAc), 169.1 (CO of OAc), 169.0 (CO of OAc), 168.8 (CO of OAc), 168.1 (CO of OAc), 168.0 (CO of OAc), 144.7 and 144.6 (CH$_2$*C*CH), 136.6 and 136.5(C$_{e/f}$), 134.0 and 133.9 (C$_{e/f}$), 119.9 and 119.7 (CH$_2$C*C*H), 85.2 (C-1), 73.0 (C-5), 69.8 and 69.7 (C-3), 67.1 and 67.0 (C-2/4), 66.0 (C-2/4), 60.3 and 60.2 (C-6), 49.4 and 49.2 (C$_{b/c}$), 47.6 (C$_{b/c}$), 47.2 (C$_g$), 45.5 and 45.3 (C$_{a/d}$), 44.1 and 44.0 (C$_{a/d}$), 34.0 and 33.9 (*C*H$_2$-triaz), 19.7 (CH$_3$ of OAc), 19.6 (CH$_3$ of OAc), 19.5 (CH$_3$ of OAc), 19.3 (CH$_3$ of OAc), 19.2 (CH$_3$ of OAc). IR (ATR): 3387, 2972, 1745, 1651, 1526, 1368, 1210, 1044, 923, 733 cm^{-1}. HRMS (ESI+): m/z calculated for $C_{43}H_{54}N_8O_{20}$ + H$^+$ [M + H$^+$]: 1003.3533. Found 1003.3555.

Bicyclo[2.2.1]hept-5-ene-2-*endo*-3-*exo*-2,3-dicarboxamide, *N*-(β-D-galactopyranosyl-1,2,3-triazol-4-ylmethyl) (17)

Prepared from **16** according to general acetyl ester hydrolysis procedure. White amorphous solid (242 mg, 97%). $[\alpha]_D^{19}$: 11.0° (c = 1, H_2O). ^{1}H NMR (500 MHz, D_2O) δ 8.16 (appd, J = 15.9 Hz, 2H, triaz-H), 6.33–6.28 (m, 1H, H$_e$/H$_f$), 6.05–5.99 (m, 1H, H$_e$/H$_f$), 5.68 (dd, J = 9.2, 2.3 Hz, 2H, H-1), 4.53–4.43 (m, 4H, CH_2-triaz), 4.19 (appt, J = 9.5 Hz, 2H, H-2), 4.08 (appd, J = 3.3 Hz, 2H, H-4), 3.99 (appt, J = 6.1 Hz, 2H, H-5), 3.87 (dd, J = 9.8, 3.3 Hz, 2H, H-3), 3.78 (appd, J = 6.0 Hz, 4H, H-6 and H-6′), 3.25–3.19 (m, 2H, H$_a$/H$_d$ and H$_b$/H$_c$), 3.01 (s, 1H, H$_a$/H$_d$), 2.53 (d, J = 4.1 Hz, 1H, H$_b$/H$_c$), 1.66 (d, J = 8.6 Hz, 1H, H$_g$), 1.42 (d, J = 7.6 Hz, 1H, H$_{g'}$). ^{13}C NMR (126 MHz, D_2O) δ 176.8 (CO), 175.8 (C'O), 145.2 (*C*-triaz), 138.2 (C═C), 134.6 (C═C), 123.1 (CH$_2$C*C*H), 88.2 (C-1), 78.4 (C-5), 73.0 (C-3), 69.8 (C-2), 68.7 (C-4), 60.9 (C-6), 48.6 (C$_b$/C$_c$), 48.2 (C$_a$/C$_d$), 47.8 (C$_b$/C$_c$), 47.5 (C$_g$), 46.4 (C$_a$/C$_d$), 34.6 (*C*H$_2$-triaz), 34.5 (*C*′H$_2$-triaz). IR (ATR): 3282, 2929, 1760, 1642, 1535, 1355, 1300, 1243, 1089, 1052, 986, 889 cm^{-1}. HRMS (ESI+): m/z calculated for $C_{27}H_{38}N_8O_{12}$ + Na$^+$ [M + Na$^+$]: 689.2507. Found 689.2490.

Bicyclo[2.2.1]hept-5-ene-2,3-*endo*-2,3-dicarboxamide, *N*-(prop-2-yn-1-yl) (19)

Cis-5-norbornene-2,3-*endo*-dicarboxylic acid **18** (300 mg, 1.65 mmol) and TBTU (1.323 g, 4.12 mmol) were dissolved in anhydrous DMF (15 mL) under N_2. NEt$_3$ (0.57 mL, 4.12 mmol) and propargylamine (0.22 mL, 3.46 mmol) were added after 10 min. The reaction was allowed to stir for 48 h. DMF was removed *in vacuo*, the resulting residue was dissolved in DCM (20 mL) and washed with brine (3 × 20 mL), and $NaHCO_3$ (2 × 20 mL), dried ($MgSO_4$), filtered and concentrated *in vacuo* to yield the crude product. This was then purified by silica gel column chromatography (1 : 1–1.5 : 1 EtOAc : pet. ether) to give **19**: white solid (334 mg, 79%). R_f = 0.08 (1 : 1 EtOAc : pet. ether). ^{1}H NMR (500 MHz, DMSO) δ 7.70 (t, J = 5.3 Hz, 2H, N*H*), 6.09 (t, J = 1.8 Hz, 2H, H$_e$ and H$_f$), 3.82–3.64 (m, 4H, CH_2-CCH), 3.12–3.09 (m, 2H, H$_b$ and H$_c$), 3.04 (t, J = 2.5 Hz, 2H, CH$_2$CC*H*), 2.96–2.94 (m, 2H, H$_a$ and H$_d$), 2.08 (s, 1H), 1.25–1.19 (m, 1H). ^{13}C NMR (125 MHz, DMSO) δ 171.5 (CO), 134.9 (C$_e$ and *C*$_f$), 81.9 (CH$_2$*C*CH), 73.2 (CH$_2$C*C*H), 50.1 (C$_b$ and C$_c$), 48.9 (C$_g$), 46.7 (C$_a$ and C$_d$), 28.4 (*C*H$_2$CCH). IR (ATR): 3286,

1654, 1525, 1415, 1333, 1278, 1256, 1226, 1098, 1029, 908, 846 cm^{-1}. HRMS (ESI+): *m*/*z* calculated for $C_{15}H_{16}N_2O_2 + Na^+$ [M + Na^+]: 279.1109. Found 279.1105.

Bicyclo[2.2.1]*cis*-hept-5-ene-2,3-*endo*-2,3-dicarboximide, *N*-(2,3,4,6-tetra-*O*-acetyl-β-D-galactopyranosyl-1,2,3-triazol-4-ylmethyl) (20)

Prepared from **18** and 2,3,4,6-tetra-*O*-acetyl-1-β-azido-D-galactopyranoside[34] according to general CuAAC procedure. Off-white solid (200 mg, 74%). R_f = 0.41 (DCM : MeOH 9 : 1). $[\alpha]_D^{22}$: −6.36° (*c* = 1.1, DCM). ^{1}H NMR (500 MHz, $CDCl_3$) δ 7.83 (s, 1H, triaz-H), 7.79 (s, 1H, triaz-H′), 6.97 (t, *J* = 5.5 Hz, 1H, N*H*CH_2-triaz), 6.83 (t, *J* = 5.6 Hz, 1H, N*H*CH_2-triaz), 6.27 (ddd, *J* = 35.6, 5.3, 3.0 Hz, 2H, H_e and H_f), 5.83–5.77 (m, 2H, H-1 and H-1′), 5.52–5.46 (m, 4H, H-2, H-2′, H-4 and H-4′), 5.24–5.18 (m, 2H, H-3 and H-3′), 4.42–4.01 (m, 10H, CH_2-triaz ×2, H-5, H-5′, H-6, H-6′, H-6″ and H-6‴), 3.25–3.17 (m, 2H, H_b and H_c), 3.06 (app s, 2H, H_a and H_d), 2.16 (s, 6H, OAc), 2.01–1.88 (m, 12H, OAc ×2), 1.80 (app d, 6H, OAc), 1.43–1.23 (m, 2H, H_g and $H_{g'}$). ^{13}C NMR (126 MHz, $CDCl_3$) δ 171.7 (CO), 171.7 (CO), 169.3 (CO of OAc), 169.3 (CO of OAc), 169.1 (CO of OAc), 168.9 (CO of OAc), 168.8 (CO of OAc), 167.9 (CO of OAc), 167.9 (CO of OAc), 144.6 (*C*-triaz), 144.5 (*C*-triaz), 134.6 (C═C), 134.2 (C═C), 120.4 (CH_2CCH), 120.2 (CH_2CCH), 85.1 (C-1), 72.9 (C-5), 69.9 (C-3), 67.0 (C-2/4), 65.9 (C-2/4), 60.2 (C-6), 60.1 (C-6′), 50.5 ($C_{b/c}$), 50.3 ($C_{b/c}$), 48.7 (C_g), 46.1 (C_a and C_d), 33.7 (*C*H_2-triaz), 19.7 (CH_3 of OAc), 19.6 (CH_3 of OAc), 19.6 (CH_3 of OAc), 19.5 (CH_3 of OAc), 19.2 (CH_3 of OAc). IR (ATR): 3392, 2967, 1746, 1663, 1527, 1368, 1211, 1045, 922 cm^{-1}. HRMS (ESI+): *m*/*z* calculated for $C_{43}H_{54}N_8O_{20} + Na^+$ [M + Na^+]: 1025.3352. Found 1025.3387.

Bicyclo[2.2.1]*cis*-hept-5-ene-2,3-*endo*-2,3-dicarboximide, *N*-(β-D-galactopyranosyl-1,2,3-triazol-4-ylmethyl) (21)

Prepared from **20** according to general acetyl ester hydrolysis procedure without Amberlite treatment. White amorphous solid (169 mg, 96%). $[\alpha]_D^{18}$: 14.0° (*c* = 1, H_2O). ^{1}H NMR (500 MHz, D_2O) δ 8.32 (s, 1H, triaz-H), 8.18 (s, 1H, triaz-H′), 5.89 (qd, *J* = 5.5, 3.0 Hz, 2H, H_e and H_f), 5.74 (d, *J* = 9.2 Hz, 1H, H-1), 5.68 (d, *J* = 9.2 Hz, 1H, H-1′), 4.68 (s, 4H, CH_2-triaz), 4.29–4.18 (m, 4H, H-2 and H-2′), 4.13 (dd, *J* = 3.3, 0.6 Hz, 1H, H-4), 4.11 (dd, *J* = 3.3, 0.6 Hz, 1H, H-4′), 4.06–3.99 (m, 2H, H-5 and H-5′), 3.92 (dd, *J* = 9.8, 3.3 Hz, 1H, H-3), 3.89 (dd, *J* = 9.8, 3.3 Hz, 1H, H-3′), 3.81 (appdd, *J* = 7.4, 6.2 Hz, 4H, H-6, H-6′, H-6″ and H-6‴), 3.50 (dd, *J* = 3.0, 1.5 Hz, 2H, H_b and H_c), 3.35 (dd, *J* = 2.5, 1.2 Hz, 2H, H_a and H_d), 1.67 (dt, *J* = 8.9, 1.6 Hz, 1H, H_g), 1.60 (d, *J* = 8.9 Hz, 1H, $H_{g'}$). ^{13}C NMR (126 MHz, D_2O) δ 180.8 (CO), 143.4 (*C*-triaz), 142.3 (*C*′-triaz), 134.3 (C═C), 124.0 (*C*H-triaz), 123.6 (*C*′H-triaz), 88.0 (C-1), 87.9 (C′-1), 78.4 (C-5), 78.3 (C′-5), 73.1 (C-3), 73.0 (C′-3), 69.7 (C-2), 69.7 (C′-2), 68.6 (C-4), 68.6 (C′-4), 60.9 (C-6), 60.8 (C′-6), 51.9 (C_g), 45.7 (C_b and C_c), 44.9 (C_a and C_d), 32.8 (*C*H_2CCH). IR (ATR): 3293, 2932, 1764, 1688, 1560, 1401, 1336, 1232, 1091, 1051, 886, 815, 728 cm^{-1}. HRMS (ESI+): *m*/*z* calculated for $C_{27}H_{38}N_8O_{12} + Na^+$ [M + Na^+]: 689.2507. Found 689.2501.

N-(β-D-galactopyranosyl-1,2,3-triazol-4-ylmethyl)bicylco[2.2.1]*cis*-hept-5-ene-2,3-*endo*-dicarboximide (22)

As per general acetyl ester hydrolysis procedure: *cis*-norbornene compound **20** (155 mg, 0.155 mmol) was dissolved in methanol/H_2O (4 mL, 2 mL). NEt_3 (0.1 mL) was added, and the reaction mixture was allowed to stir at 45 °C for 6 h. The solution was cooled, Amberlite H^+ was added and the mixture was allowed to stir for 30 min. The solution was filtered and the solvent was removed *in vacuo*. Monovalent-imide analogue **22** was formed: white amorphous solid (63 mg, 100%). $[\alpha]_D^{26}$: 5° (*c* = 1.2, MeOH). ^{1}H NMR (500 MHz, D_2O) δ 8.10 (s, 1H, triaz-H), 5.82 (qd, *J* = 5.5, 3.0 Hz, 2H, H_e and H_f), 5.60 (d, *J* = 9.2 Hz, 1H, H-1), 4.61 (s, 2H, CH_2-triaz), 4.13 (t, *J* = 9.5 Hz, 1H, H-2), 4.03 (dd, *J* = 3.3, 0.7 Hz, 1H, H-4), 3.93 (td, *J* = 6.0, 0.8 Hz, 1H, H-5), 3.81 (dd, *J* = 9.8, 3.3 Hz, 1H, H-3), 3.72 (d, *J* = 6.1 Hz, 2H, H-6 and H-6′), 3.44–3.41 (m, 2H, H_b and H_c), 3.28–3.26 (m, 2H, H_a and H_d), 1.62–1.49 (m, 2H, H_g and $H_{g'}$). ^{13}C NMR (125 MHz, D_2O) δ 180.8 (CO), 142.4 (CH_2CCH), 134.3 (C_e and C_f), 124.1 (CH_2CCH), 88.0 (C-1), 78.4 (C-5), 73.1 (C-3), 69.8 (C-2), 68.7 (C-4), 60.9 (C-6), 52.0 (C_g), 45.8 (C_b and C_c), 45.0 (C_a and C_d), 32.9 (*C*H_2-CCH). IR (ATR): 3346, 2943, 1765, 1686, 1399, 1336, 1168, 1091, 1050, 883, 727 cm^{-1}. HRMS (ESI+): *m*/*z* calculated for $C_{18}H_{22}N_4O_7 + Na^+$ [M + Na^+]: 429.1386. Found 429.1362.

Chemistry computational methods

Geometry optimisations. Initial conformational searching of compounds **1** and **21** was carried out with the conformer-rotamer ensemble sampling tool utility (crest, version 2.7) based on the GFN2-xTB method, as implemented in the xtb (version 6.1) code.[53,54] The default iterative version of the MTD-GC routine (iMTD-GC) was utilized to generate a complete conformer ensemble.[55] This workflow performs several independent metadynamics (MTD) simulations at *T* = 300 K utilizing a history-dependent biasing potential with different parameters for the potential. The collective variables are defined as previous minima in the conformational space, expressed as root-mean-square-deviation (RMSD) between the structures. Snapshots are then geometry optimized in a multi-level filtering procedure applying energy windows of 15, 10, and 6 kcal mol^{-1}, respectively. Regular molecular dynamics (MD) simulations are carried out to sample rotameric structures, and in the final step a genetic *z*-matrix crossing (GC) procedure is applied in order to filter out identical geometries. For the complete sampling a generalized Born model with solvent accessible surface area (GBSA) was invoked to account for the effect of water solvent and prevent electrostatic collapse of the molecules. Subsequent full geometry optimizations on the final conformer ensemble were performed with the Gaussian 09 (revision E.01) program.[56] All geometries were fully optimized with the B3PW91 functional[57,58] in conjunction with the 6-31G(d,p) basis set on all atoms.[59,60] Subsequent vibrational frequency calculations on optimized geometries were utilized to confirm that each structure represents a true minimum on

the potential energy surface. Dispersion effects were not explicitly taken into account during geometry optimizations, since initial optimizations of low-energy conformers of **1** invoking Grimme's empirical D3 dispersion correction[61,62] resulted in highly globular structures (see Fig. S2†).[63] Such structures appear to result from maximizing intramolecular H-bonding and dispersion interactions. They represent the closest packing conformers that are possible for this molecule, which are, however, more unlikely to exist in solution. Solvent effects were here only crudely approximated by performing all geometry optimizations in the presence of a reaction field using the integral equation formalism model (IEFPCM) in combination with the radii and non-electrostatic terms for the SMD solvation model.[64] The employed dielectric constant (ϵ = 78.35) and related solvent parameters correspond to those of water. Subsequent single point calculations were then performed on optimised geometries including the dispersion correction term, *i.e.* at the SMD-B3PW91-D3/6-31G** level of theory. Additional high-level single point calculations employed the DSD-PBEP86-D3 (ref. 65) double-hybrid functional as well as the DLPNO-CCSD(T)[66] level of theory, as implemented in ORCA (version 4.2.1).[67] Both methods were used in conjunction with the def2-TZVPP[68] basis set and the RIJK approximation for Coulomb and HF exchange integrals, as well as the RI approximation for integral transformations in the MP2 and DLPNO modules. These approximations require the def2-TZVPP/C[69] and def2/JK[70] auxiliary basis sets.

Metadynamics simulations. After a preliminary minimization, each of the two systems (**1** and **21**) was subjected to well-tempered metadynamics simulations,[71,72] utilizing the ABIN (version 1.1)[73] molecular dynamics software in conjunction with the PLUMED (version 2.6.0) plugin.[74] Forces and energies were obtained externally by interfacing to the GFN1-xTB code (invoking the GBSA model for water solvent). These simulations employed a Nosé–Hoover[75–77] thermostat at a temperature of 298.15 K, using a time step of 20 au (~0.5 fs). For each system, two collective variables (CV1 and CV2 respectively) were defined as torsional angles (see Fig. S5† for definition). After a first trial phase where the simulation parameters were tuned properly, the Gaussian width for both CVs was set to 0.35 radians, spawned every 500 steps. A Gaussian height of 1.2 kJ mol^{-1} and a biasfactor of 6.0 was used in all cases. In order to sample the conformational space efficiently, 40 multiple walkers were run in parallel during the simulation. The deposited bias is shared along all replicas (disk-based sharing) so that the history-dependent potential depends on the full history. The free energy surfaces (FESs) were obtained from the combined bias potential from all trajectories as calculated with respect to the two CVs.

QM/MM simulations with explicit solvation. QM/MM molecular dynamics was carried out at the GFN1-xTB/TIP3P level of theory using a modified version of Chemshell (version 3.7),[78,79] The QM-region was calculated using an interface to the xTB code, whilst the MM region was evaluated with the DL_POLY[80] code as implemented in Chemshell. A 33 Å radius sphere of TIP3P water molecules had the molecule inserted into the center. An outer frozen layer of 4 Å was defined to avoid solvent evaporation and a spherical boundary potential of 3 E_h/Bohr^2 (acting 1 Å into the frozen layer) was used to avoid active water molecules diffusing through the frozen layer. Another short-range spherical potential (3 E_h/Bohr^2) was applied to keep the molecule centred during the dynamics. A timestep of 1 fs was used to integrate Newton's equations of motion using the leapfrog algorithm where the masses of all hydrogen atoms were substituted for deuterium masses. A Nosé–Hoover 4-chain thermostat with a time constant of 0.02 ps was used to maintain a temperature of 300 K. The QM/MM Hamiltonian used electrostatic embedding (TIP3P[81] pointcharges polarizing the GFN1-xTB Hamiltonian) and Lennard-Jones potentials were used to describe the short-range interactions between QM and MM molecules (OPLS-AA[82] parameters were used for the molecules from the LigParGen[83] webserver). This simulation setup takes advantage of affordable semiempirical QM/MM molecular dynamics, and has already been successfully applied to other systems.[84] 100 ps QM/MM MD simulations were performed. Trajectories of all molecular dynamics simulations were processed with the VMD (version 1.9.2) package.[85,86]

Biology

Fungal strain. *C. albicans* (MEN, serotype B, clinical isolate from a corneal infection) was maintained on sabouraud dextrose agar and cultures were grow to the stationary phase (1–2 × 10^8 cells per mL) overnight in YEPD broth (1% (w/v) yeast extract, 2% (w/v) bacteriological peptone, 2% (w/v) glucose) at 30 °C and 200 rpm. Stationary phase yeast cells were harvested, washed with PBS and resuspended at a density of 1 × 10^8 cells per mL in PBS.

Buccal epithelial cells. Buccal epithelial cells (BECs) were harvested from healthy volunteers by gently scraping the inside of the cheek with a sterile tongue depressor. Cells were washed in PBS and resuspended at a density of 5 × 10^5 cells per mL.

Adherence assays. Yeast cells were mixed with 50 : 1 (yeast : BEC) in a final volume of 2 mL and incubated at 30 °C and 200 rpm for 90 min. The BEC/yeast cell mixture was harvested by passing through a polycarbonate membrane containing 30 μm pores which trapped the BECs but allowed unattached yeast cells to pass through. This was washed ×2 with 10 mL PBS and cells remaining on the membrane were collected and placed on glass slides which were left to air dry overnight. The cells were heat fixed and stained using 0.5% (w/v) crystal violet, rinsed using cold water to remove any surplus stain and left to air dry for 30 min. The number of *C. albicans* cells adhering to a sample of 200 BECs per treatment was assessed microscopically. In the exclusion assay the yeast cells were incubated for 90 min in the presence of each compound at the given concentration. After this time the yeast cells were harvested and washed twice with PBS before

being resuspended in 1 mL PBS before being mixed with BECs (as described). In the competition assay format yeast cells, BECs and compound (at the given concentration) were co-incubated for 90 min prior to harvesting. In the displacement assay adherence was allowed to occur by mixing the yeast cells and BECs together. BECs and adherent yeast cells were harvested and re-incubated with the compound (at the given concentration) for a further 90 min after which time the level of adherence was measured.

Statistics. All experiments were performed on three independent occasions. In each assay the number of yeast cells adhering to 200 randomly chosen BECs was determined. Results are mean ± SEM.

Ethical statement

All experiments were performed in accordance with the guidelines stipulated in Directive 2004/23/EC of the European Parliament and of the Council (31 March 2004). Experiments were approved by the Ethics Committee at Maynooth University. Informed consents were obtained from human participants of this study.

Conflicts of interest

The authors declare no conflict of interest.

Acknowledgements

We would like to thank Maynooth University for the provision of the John and Pat Hume Scholarship for H. Martin. We would like to thank Dr. Elisa Fadda (Maynooth University) for assistance with initial geometry optimization calculations.

References

1 D. H. Stones and A. M. Krachler, *Biochem. Soc. Trans.*, 2016, **44**, 1571–1580.
2 K. A. Kline, S. Fälker, S. Dahlberg, S. Normark and B. Henriques-Normark, *Cell Host Microbe*, 2009, **5**, 580–592.
3 F. Ilaria and F. Giusti, EM Reconstruction of Adhesins: Future Prospects, in *Bacterial Adhesion. Advances in Experimental Medicine and Biology*, ed. D. Linke and A. Goldman, Springer, Dordrecht, 2011, pp. 271–284.
4 V. Krishnan and S. V. L. Narayana, Crystallography of Gram-Positive Bacterial Adhesins, in *Bacterial Adhesion. Advances Experimental Medicine and Biology*, ed. D. Linke and A. Goldman, Springer, Dordrecht, 2011, pp. 175–195.
5 S. Fushinobu, *Acta Crystallogr., Sect. F: Struct. Biol. Commun.*, 2018, **74**, 473–479.
6 A. Audfray, A. Varrot and A. Imberty, *C. R. Chim.*, 2013, **16**, 482–490.
7 S. Cecioni, A. Imberty and S. Vidal, *Chem. Rev.*, 2015, **115**, 525–561.
8 V. Lehot, Y. Brissonnet, C. Dussouy, S. Brument, A. Cabanettes, E. Gillon, D. Deniaud, A. Varrot, P. Le Pape and S. G. Gouin, *Chem. – Eur. J.*, 2018, **24**, 19243.
9 V. Denavit, D. Lainé, C. Bouzriba, E. Shanina, É. Gillon, S. K. Buffet, I. Nierengarten, N. Galanos, E. Gillon, M. Holler, A. Imberty, S. E. Matthews, S. Vidal, S. P. Vincent and J. F. Nierengarten, *Chem. – Eur. J.*, 2016, **22**, 2955–2963.
10 F. Pertici, N. J. de Mol, J. Kemmink and R. J. Pieters, *Chem. – Eur. J.*, 2013, **19**, 16923–16927.
11 G. Michaud, R. Visini, M. Bergmann, G. Salerno, R. Bosco, E. Gillon, B. Richichi, C. Nativi, A. Imberty, A. Stocker, T. Darbre and J. L. Reymond, *Chem. Sci.*, 2016, **7**, 166–182.
12 W. Schönemann, J. Cramer, T. Mühlethaler, B. Fiege, M. Silbermann, S. Rabbani, P. Dätwyler, P. Zihlmann, R. P. Jakob, C. P. Sager, M. Smieško, O. Schwardt, T. Maier and B. Ernst, *ChemMedChem*, 2019, **14**, 749–757.
13 A. Saragliadis and D. Linke, *Cell Surf.*, 2019, **5**, 100025.
14 A. Fazly, C. Jain, A. C. Dehner, L. Issi, E. A. Lilly, A. Ali, H. Cao, P. L. Fidel Jr., R. P. Rao and P. D. Kaufman, *Proc. Natl. Acad. Sci. U. S. A.*, 2013, **110**, 13594–13599.
15 C. J. Nobile and A. D. Johnson, *Annu. Rev. Microbiol.*, 2015, **69**, 71–92.
16 C. Spampinato and D. Leonardi, *BioMed Res. Int.*, 2013, **2013**, 204237.
17 P. Southern, J. Horbul, D. Maher and D. A. Davis, *PLoS One*, 2008, **3**, e2067.
18 S. A. Nikou, N. Kichik, R. Brown, N. O. Ponde, J. Ho, J. R. Naglik and J. P. Richardson, *Pathogens*, 2019, **8**, 53.
19 R. A. Calderone and W. A. Fonzi, *Trends Microbiol.*, 2001, **9**, 327–335.
20 D. L. Moyes, J. P. Richardson and J. R. Naglik, *Virulence*, 2015, **6**, 338–346.
21 P. Sundstrom, *Cell. Microbiol.*, 2002, **4**, 461–469.
22 B. Wächtler, D. Wilson, K. Haedicke, F. Dalle and B. Hube, *PLoS One*, 2011, **6**, e17046.
23 W. L. Chaffin, J. L. López-Ribot, M. Casanova, D. Gozalbo and J. P. Martínez, *Microbiol. Mol. Biol. Rev.*, 1998, **62**, 130–180.
24 R. G. Willaert, *J. Fungi*, 2018, **4**, 119.
25 F. S. Ielasi, K. Decanniere and R. G. Willaert, *Acta Crystallogr., Sect. D: Biol. Crystallogr.*, 2012, **68**, 210–217.
26 M. Maestre-Reyna, R. Diderrich, M. S. Veelders, G. Eulenburg, V. Kalugin, S. Brückner, P. Keller, S. Rupp, H. U. Mösch and L. O. Essen, *Proc. Natl. Acad. Sci. U. S. A.*, 2012, **109**, 16864–16869.
27 D. S. Donohue, F. S. Ielasi, K. V. Y. Goossens and R. G. Willaert, *Mol. Microbiol.*, 2011, **80**, 1667–1679.
28 F. S. Ielasi, M. Alioscha-Perez, D. Donohue, S. Claes, H. Sahli, D. Schols and R. G. Willaert, *mBio*, 2016, **7**(4), e00584-16.
29 A. Varrot, S. M. Basheer and A. Imberty, *Curr. Opin. Struct. Biol.*, 2013, **23**, 678–685.
30 H. Martin, M. Mc Govern, L. Abbey, A. Gilroy, S. Mullins, S. Howell, K. Kavanagh and T. Velasco-Torrijos, *Eur. J. Med. Chem.*, 2018, **160**, 82–93.
31 V. V. Levterov, Y. Panasyuk, V. O. Pivnytska and P. K. Mykhailiuk, *Angew. Chem., Int. Ed.*, 2020, **59**, 7161–7167.
32 M. Kunishima, C. Kawachi, J. Monta, K. Terao, F. Iwasaki and S. Tani, *Tetrahedron*, 1999, **55**, 13159–13170.

33 J. Weyrauch, A. Hashmi, A. Schuster, T. Hengst, S. Schetter, A. Littmann, M. Rudolph, M. Hamzic, J. Visus, F. Rominger, W. Frey and J. Bats, *Chem. – Eur. J.*, 2010, **16**, 956–963.

34 F. D. Tropper, F. O. Andersson, S. Braun and R. Roy, *Synthesis*, 1992, **1992**, 618–620.

35 R. I. Storer, C. Aciro and L. H. Jones, *Chem. Soc. Rev.*, 2011, **40**, 2330–2346.

36 L. A. Marchetti, L. K. Kumawat, N. Mao, J. C. Stephens and R. B. P. Elmes, *Chem*, 2019, **5**, 1398–1485.

37 P. Chauhan, S. Mahajan, U. Kaya, D. Hack and D. Enders, *Adv. Synth. Catal.*, 2015, **357**, 253–281.

38 F. R. Wurm and H. A. Klok, *Chem. Soc. Rev.*, 2013, **42**, 8220–8236.

39 A. A. Karelin, Y. E. Tsvetkov, L. Paulovičová, S. Bystrický, E. Paulovičová and N. E. Nifantiev, *Carbohydr. Res.*, 2009, **344**, 29–35.

40 T. K. Lindhorst, K. Bruegge, A. Fuchs and O. Sperling, *Beilstein J. Org. Chem.*, 2010, **6**, 801–809.

41 O. Sperling, A. Fuchs and T. K. Lindhorst, *Org. Biomol. Chem.*, 2006, **4**, 3913–3922.

42 O. Sperling, M. Dubber and T. K. Lindhorst, *Carbohydr. Res.*, 2007, **342**, 696–703.

43 S. Roy, M. Barrera-Tomas and D. Giguere, Squaric Acid Diethyl Ester-Mediated Homodimerization of Unprotected Carbohydrates, in *Carbohydrate Chemistry: Proven Synthetic Methods*, ed. R. Roy and S. Vidal, CRC Press, Boca Raton, 1st edn, 2015, vol. 3, pp. 107–112.

44 J. Ramos, S. Arufe, H. Martin, D. Rooney, R. B. P. Elmes, A. Erxleben, R. Moreira and T. Velasco-Torrijos, *Soft Matter*, 2020, DOI: 10.1039/D0SM01075H.

45 S. Lamande-Langle, C. Collet, R. Hensienne, C. Vala, F. Chretien, Y. Chapleur, A. Mohamadi, P. Lacolley and V. Regnault, *Bioorg. Med. Chem.*, 2014, **22**, 6672–6683.

46 J. P. Chinta and C. P. Rao, *Carbohydr. Res.*, 2013, **369**, 58–62.

47 S. Sutthasupa, M. Shiotsuki, H. Matsuoka, T. Masuda and F. Sanda, *Macromolecules*, 2010, **43**, 1815–1822.

48 K. H. Mortell, R. V. Weatherman and L. L. Kiessling, *J. Am. Chem. Soc.*, 1996, **118**, 2297–2298.

49 M. D. Johnstone, E. K. Schwarze, G. H. Clever and F. M. Pfeffer, *Chem. – Eur. J.*, 2015, **21**, 3948–3955.

50 J. R. Engstrom, A. J. Savyasachi, M. Parhizkar, A. Sutti, C. S. Hawes, J. M. White, T. Gunnlaugsson and F. M. Pfeffer, *Chem. Sci.*, 2018, **9**, 5233–5241.

51 A. J. Lowe, G. A. Dyson and F. M. Pfeffer, *Org. Biomol. Chem.*, 2007, **5**, 1343–1346.

52 S. M. Hickey, T. D. Ashton, G. Boer, C. A. Bader, M. Thomas, A. G. Elliott, C. Schmuck, H. Y. Yu, J. Li, R. L. Nation, M. A. Cooper, S. E. Plush, D. A. Brooks and F. M. Pfeffer, *Eur. J. Med. Chem.*, 2018, **160**, 9–22.

53 N. Foloppe and I. J. Chen, *Curr. Med. Chem.*, 2009, **16**, 3381–3413.

54 S. Grimme, C. Bannwarth, S. Dohm, A. Hansen, J. Pisarek, P. Pracht, J. Seibert and F. Neese, *Angew. Chem., Int. Ed.*, 2017, **56**, 14763–14769.

55 C. Bannwarth, S. Ehlert and S. Grimme, *J. Chem. Theory Comput.*, 2019, **15**, 1652–1671.

56 S. Grimme, *J. Chem. Theory Comput.*, 2019, **15**, 2847–2862.

57 M. J. Frisch, G. W. Trucks, H. B. Schlegel, G. E. Scuseria, M. A. Robb, J. R. Cheeseman, G. Scalmani, V. Barone, B. Mennucci, G. A. Petersson, H. Nakatsuji, M. Caricato, X. Li, H. P. Hratchian, A. F. Izmaylov, J. Bloino, G. Zheng, J. L. Sonnenberg, M. Hada, M. Ehara, K. Toyota, R. Fukuda, J. Hasegawa, M. Ishida, T. Nakajima, Y. Honda, O. Kitao, H. Nakai, T. Vreven, J. A. Montgomery Jr., J. E. Peralta, F. Ogliaro, M. Bearpark, J. J. Heyd, E. Brothers, K. N. Kudin, V. N. Staroverov, R. Kobayashi, J. Normand, K. Raghavachari, A. Rendell, J. C. Burant, S. S. Iyengar, J. Tomasi, M. Cossi, N. Rega, J. M. Millam, M. Klene, J. E. Knox, J. B. Cross, V. Bakken, C. Adamo, J. Jaramillo, R. Gomperts, R. E. Stratmann, O. Yazyev, A. J. Austin, R. Cammi, C. Pomelli, J. W. Ochterski, R. L. Martin, K. Morokuma, V. G. Zakrzewski, G. A. Voth, P. Salvador, J. J. Dannenberg, S. Dapprich, A. D. Daniels, Ö Farkas, J. B. Foresman, J. V. Ortiz, J. Cioslowski and D. J. Fox, *Gaussian 09 (Revision E.01)*, Gaussian Inc., Wallingford, CT, 2009.

58 A. D. Becke, *Phys. Rev. A: At., Mol., Opt. Phys.*, 1988, **38**, 3098–3100.

59 A. D. Becke, *J. Chem. Phys.*, 1993, **98**, 5648–5652.

60 R. Ditchfield, W. J. Hehre and J. A. Pople, *J. Chem. Phys.*, 1971, **54**, 724.

61 P. C. Hariharan and J. A. Pople, *Theor. Chem. Acc.*, 1973, **28**, 213–222.

62 S. Grimme, J. Antony, S. Ehrlich and H. Krieg, *J. Chem. Phys.*, 2010, **132**, 154104.

63 S. Grimme, S. Ehrlich and L. Goerigk, *J. Comput. Chem.*, 2011, **32**, 1456–1465.

64 C.-W. von der Lieth, M. Frank and T. K. Lindhorst, *Rev. Mol. Biotechnol.*, 2002, **90**, 311–337.

65 A. V. Marenich, C. J. Cramer and D. G. Truhlar, *J. Phys. Chem. B*, 2009, **113**, 6378–6396.

66 S. Kozuch and J. M. L. Martin, *Phys. Chem. Chem. Phys.*, 2011, **13**, 20104–20107.

67 Y. Guo, C. Riplinger, U. Becker, D. G. Liakos, Y. Minenkov, L. Cavallo and F. Neese, *J. Chem. Phys.*, 2018, **148**, 011101.

68 F. Neese, *Wiley Interdiscip. Rev.: Comput. Mol. Sci.*, 2017, **8**, e1327.

69 F. Weigend and R. Ahlrichs, *Phys. Chem. Chem. Phys.*, 2005, **7**, 3297–3305.

70 A. Hellweg, C. Hättig, S. Höfener and W. Klopper, *Theor. Chem. Acc.*, 2007, **117**, 587–597.

71 F. Weigend, *J. Comput. Chem.*, 2008, **29**, 167–175.

72 A. Laio and M. Parrinello, *Proc. Natl. Acad. Sci. U. S. A.*, 2002, **99**, 12562–12566.

73 A. Barducci, G. Bussi and M. Parrinello, *Phys. Rev. Lett.*, 2008, **100**, 020603.

74 D. Hollas, J. Suchan, O. Svoboda, M. Ončák and P. Slavíček, *ABIN (version 1.1)*, https://github.com/PHOTOX/ABIN, (accessed 14 April 2020).

75 G. A. Tribello, M. Bonomi, D. Branduardi, C. Camilloni and G. Bussi, *Comput. Phys. Commun.*, 2014, **185**, 604–613.

76 S. Nosé, *Mol. Phys.*, 1984, **52**, 255–268.

77 W. G. Hoover, *Phys. Rev. A: At., Mol., Opt. Phys.*, 1985, **31**, 1695–1697.
78 G. J. Martyna, M. L. Klein and M. Tuckerman, *J. Chem. Phys.*, 1992, **97**, 2635–2643.
79 P. Sherwood, A. H. de Vries, M. F. Guest, G. Schreckenbach, C. R. A. Catlow, S. A. French, A. A. Sokol, S. T. Bromley, W. Thiel, A. J. Turner, S. Billeter, F. Terstegen, S. Thiel, J. Kendrick, S. C. Rogers, J. Casci, M. Watson, F. King, E. Karlsen, M. Sjøvoll, A. Fahmi, A. Schäfer and C. Lennartz, *J. Mol. Struct.: THEOCHEM*, 2003, **632**, 1–28.
80 S. Metz, J. Kästner, A. A. Sokol, T. W. Keal and P. Sherwood, *WIREs Comput. Mol. Sci.*, 2014, **4**, 101–110.
81 W. Smith, C. W. Yong and P. M. Rodger, *Mol. Simul.*, 2002, **28**, 385–471.
82 W. L. Jorgensen, J. Chandrasekhar, J. D. Madura, R. W. Impey and M. L. Klein, *J. Chem. Phys.*, 1983, **79**, 926–935.
83 W. L. Jorgensen, D. S. Maxwell and J. Tirado-Rives, *J. Am. Chem. Soc.*, 1996, **118**, 11225–11236.
84 L. S. Dodda, I. Cabeza de Vaca, J. Tirado-Rives and W. L. Jorgensen, *Nucleic Acids Res.*, 2017, **45**, W331–W336.
85 C. M. Sterling and R. Bjornsson, *J. Chem. Theory Comput.*, 2019, **15**, 52–67.
86 W. Humphrey, A. Dalke and K. Schulten, *J. Mol. Graphics*, 1996, **14**, 33–38.